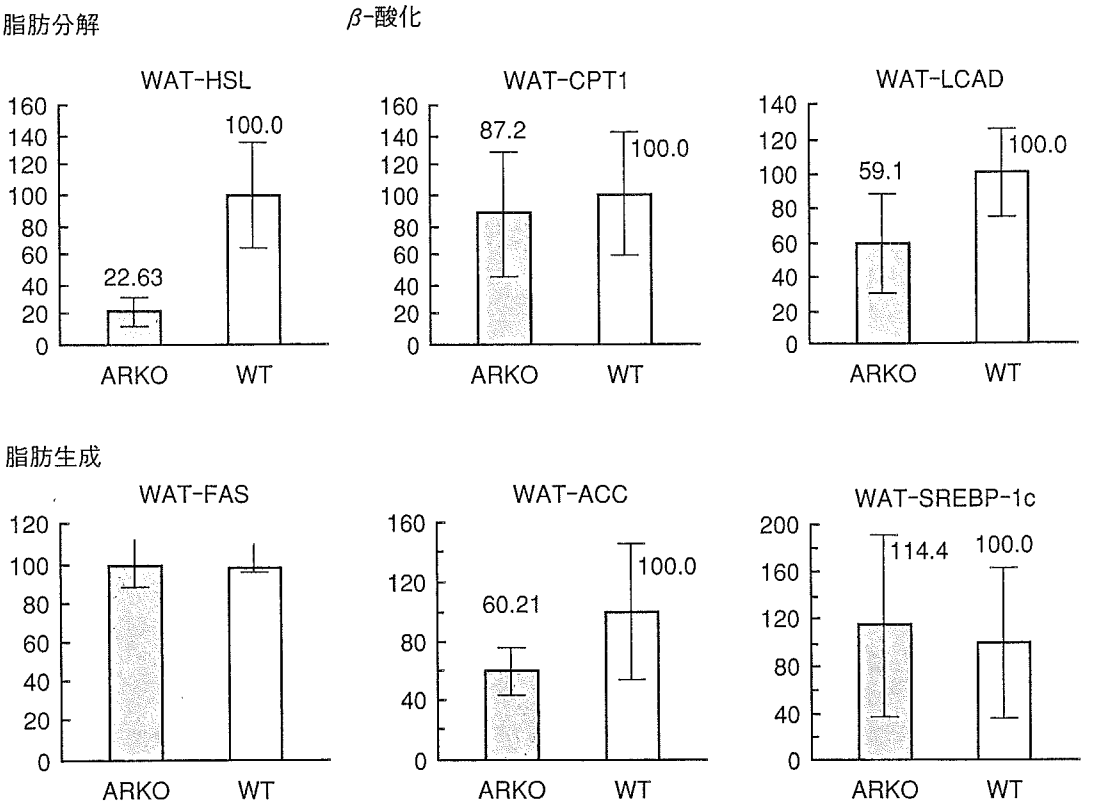

図3　雄アンドロゲン受容体ノックアウトマウスにおける脂肪分解と脂肪生成

る点とは大きく異なっていた。また，エネルギー消費の悪化という点に注目して，UCP1の発現について検討した結果では，ARKOは白色脂肪組織(WAT)で著しく発現が低下していることがわかった。これはアンドロゲン受容体の発現が褐色脂肪組織(BAT)よりもWATで高いことに関係しているものと考えられた(**図4**)。UCP1のプロモーター領域にはアンドロゲン受容体に反応するエレメントがあり，解析した範囲ではUCP1プロモーター活性がDHT(dihydrotestosterone)依存性に上昇することがわかったので，われわれはおそらくアンドロゲンのターゲット遺伝子として働いているものと考えている。

インスリン抵抗性の観点からの検討では，肥満を有するARKOでは低いと予想された血中のアディポネクチン濃度が高く，転写に関しては予想どおり低いことがわかった(**図5**)。この乖離はアディポネクチンの分泌亢進を示すもので，テストステロンがアディポネクチン分泌を抑制するという下村らの報告とも一致した結果であると考えられた。なお，血糖やインスリンには差を認めなかった。インスリンチャレンジテストや糖負荷試験の結果では肥満にかかわらずインスリン感受性に変化は認められず，アディポネクチンの関与が示唆された。また，PPARγ発現は脂肪組織で野生型に比べて相対的に低く，インスリン抵抗性を呈さないことにも関係しているのではないかと推察された。

アンドロゲンが筋肉で活発に働くことから，代表的インスリン感受性組織である骨格筋において，糖輸送蛋白や糖酸化系酵素を検討した(**図6**)。その結果，GLUT4発現が非常に高く，糖代謝に関連してHK1(hexokinase 1)の高値が認められた。糖の酸化も糖輸送も亢進していることからARKOではインスリン感受性がよいことが示唆されるが，これがアンドロゲンの直接的作用であるのか，アディポネクチンやPPARγを介した作用であるのかは現時点では明らかではない。

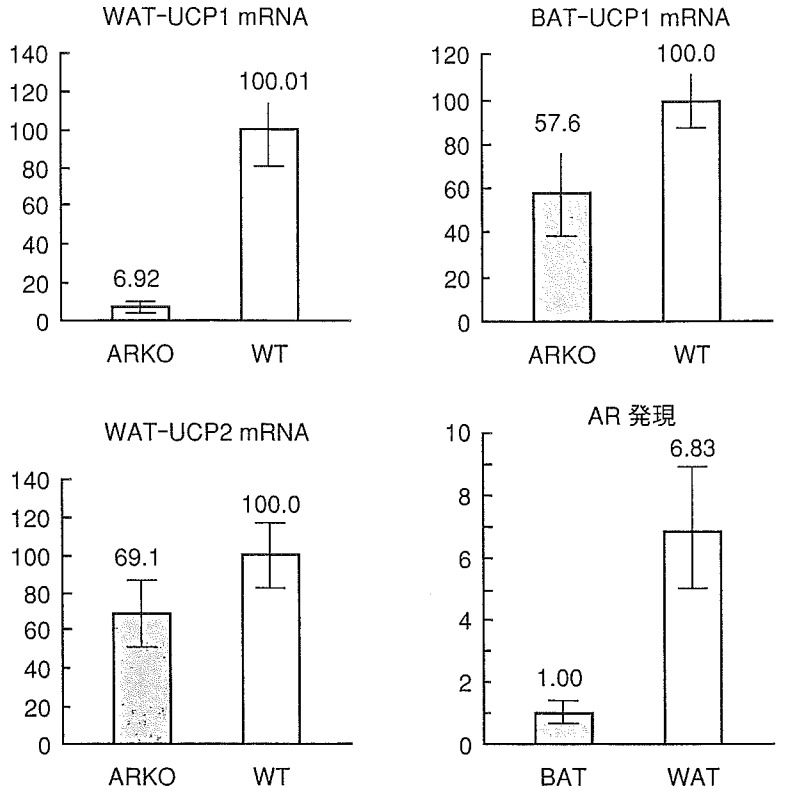

図4　雄アンドロゲン受容体ノックアウトマウスの白色脂肪組織におけるUCP1の発現低下

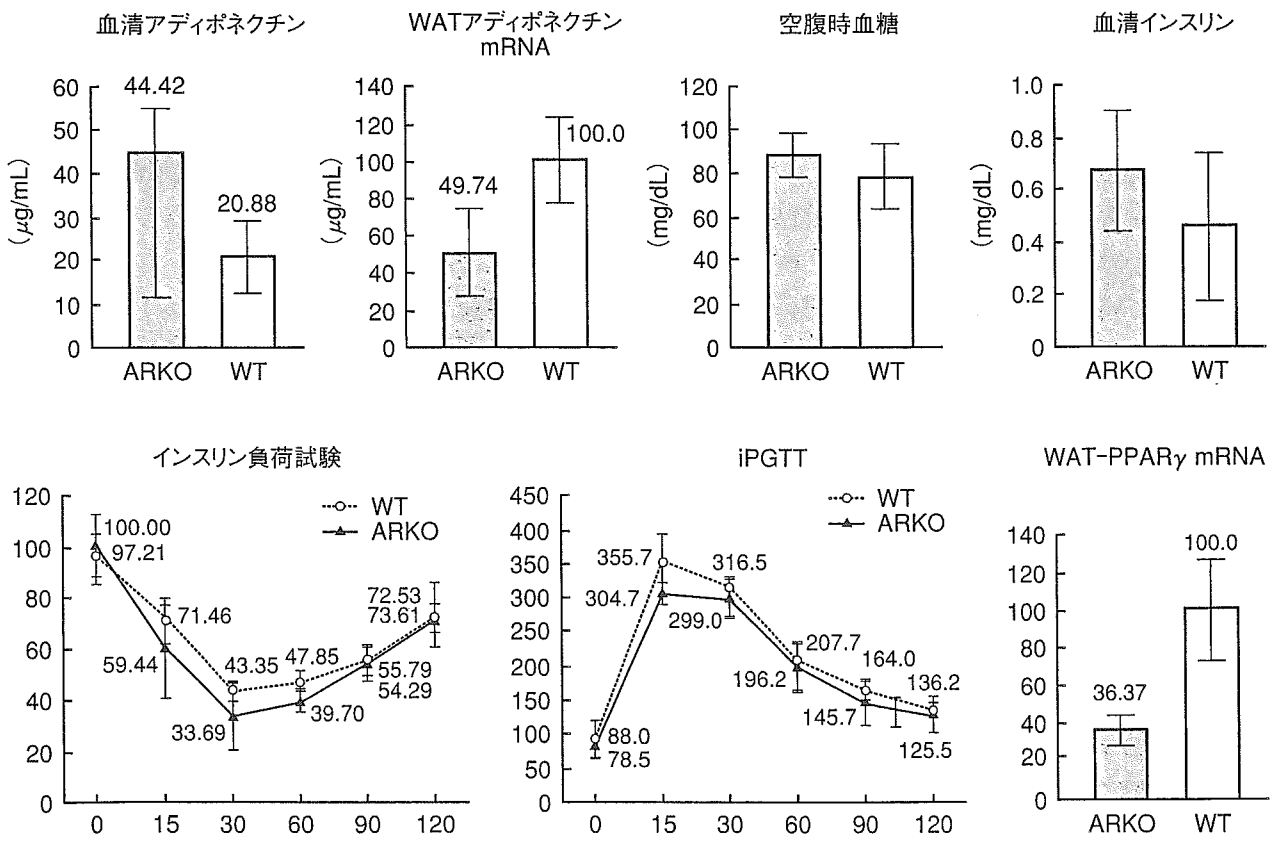

図5　雄アンドロゲン受容体ノックアウトマウスにおけるアディポネクチン分泌とインスリン感受性

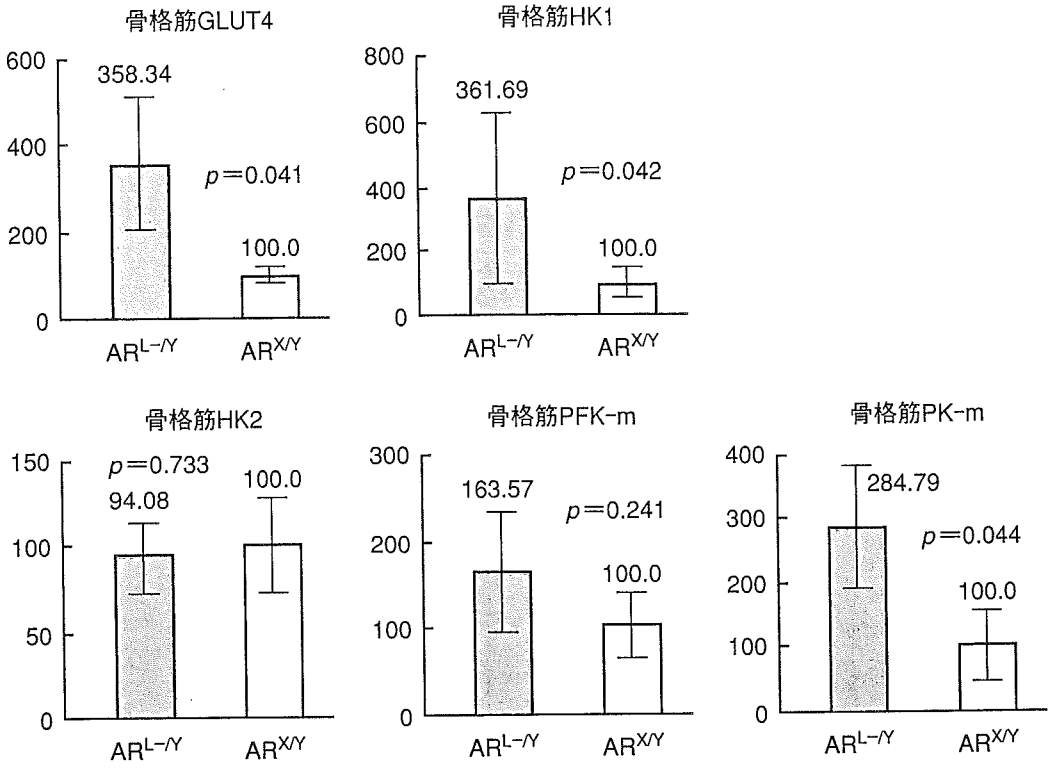

図6　雄アンドロゲン受容体ノックアウトマウスの骨格筋における糖輸送蛋白と糖代謝系酵素の発現

まとめると，雄ARKOでは晩発性の肥満を起こし，その原因の一つとしてエネルギー消費の低下が考えられた。雄ARKOの食餌摂取量は正常で運動量と酸素消費量の低下を認めた。雄ARKOの白色脂肪で認められたUCP1の発現低下が，エネルギー消費低下の一因と考えられた。肥満の原因として脂肪分解系酵素の発現低下が認められた。雄ARKOは肥満であるにもかかわらずインスリン抵抗性を認めなかった。その原因として，アディポネクチンの分泌亢進やPPARγの発現低下の関与が考えられた。

臨床での検討

ヒト男性が中年になって太ってくることに内因性テストステロンが関与しているかどうかは明らかでない。しかし現在，男性更年期が話題になっており，日本人成人男子における遊離テストステロンの正常値を最近，設定した。1,143人を対象に検討を行い基準値を決めたところ，50代以上で基準値以上の場合，有意に肥満度が高いことがわかり，生理的レベルのテストステロン値の変動が，中年期の体脂肪増加と関連している可能性が示唆された。

今後の検討

雄ARKOマウスではエネルギー消費が低下していたが，中枢性の関与については現状ではよくわかっていない。現在われわれはアンドロゲン受容体が視床下部や，脳のその他の部位のどこで染色されるか検討中である。雄性行動に関与する前視床下部やSCNでの発現が高く，これらの特徴は雌やARKOには認められないことから，何らかの形で雄特異的に肥満をきたすメカニズムへの関与が想定され，現在検討中である。

特集
Aging male
Late-onset hypogonadism/PADAMという立場から
Geriat. Med. 43(2)：197～201, 2005

Aging maleにおける肥満
(visceral obesityを中心に)

柳瀬　敏彦*　　名和田　新*

KEY WORD
テストステロン
内臓脂肪
インスリン抵抗性
androgen receptor

POINT
- 内因性のテストステロンは体脂肪の増加を防ぐ方向に作用する．
- 内因性のテストステロンもインスリン抵抗性を増大させる方向に作用している可能性がある．
- 中高年以降のいわゆる「中年太り」や生活習慣病の発症要因の一因として，加齢に伴うテストステロンの低下や作用不全が関与している可能性がある．

0387-1088/05/¥500/論文/JCLS

はじめに

性ステロイドはメタボリックシンドロームの性差を説明する重要な背景因子であるが，研究成績は比較的少ない．一般に男性では中高年以降，上半身型の脂肪蓄積パターンを示すようになり，メタボリックシンドロームの発症リスクの増大と関連する．この背景要因には，加齢に伴う性ステロイド，すなわちテストステロンの低下変動がその一因として関与する可能性が考えられる．またテストステロンの合成障害や作用不全を示すヒトの病態やモデル動物において，白色脂肪組織(white adipose tissue：WAT)重量の増加に伴う内臓脂肪型肥満が存在することが明らかにされてきている．

本稿ではテストステロンと体脂肪の関連に関する最近の研究の進展について，エストロゲンに関する同様の研究に関しても対比として交えながら紹介する．

*やなせ　としひこ，なわた　はじめ：九州大学大学院医学研究院病態制御内科

テストステロン

近年，テストステロンが，男性における体構成を決める重要な因子であるとする成績が蓄積されつつある．男性において脂肪蓄積の程度は血中テストステロン値と逆相関するとの成績を認める[1]．われわれは腹部臍高のCT断面のV/S比の評価による男性の内臓脂肪の割合も加齢とともに増加することを認めた(図1)．一方，性腺機能低下症の男性では，加齢とともに体脂肪の有意の増加を認め，それはテストステロンの投与によって減少することが報告されている(図2)[2]．さらに，若年健康成人の内因性血中テストステロンレベルをゴナドトロピン放出ホルモンアナログの投与によって低下させた場合

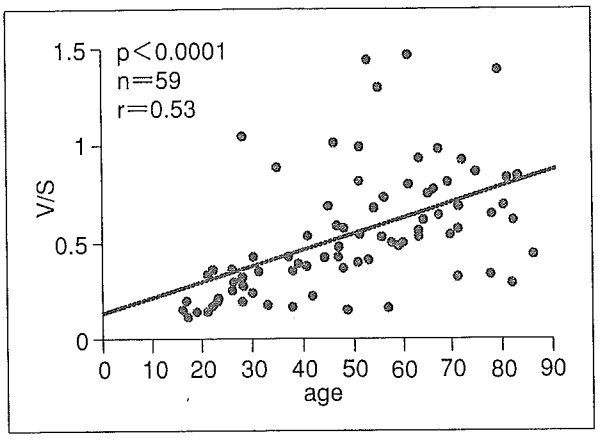

図1　男性の内臓脂肪/皮下脂肪(V/S)比に及ぼす年齢の影響(自験成績)

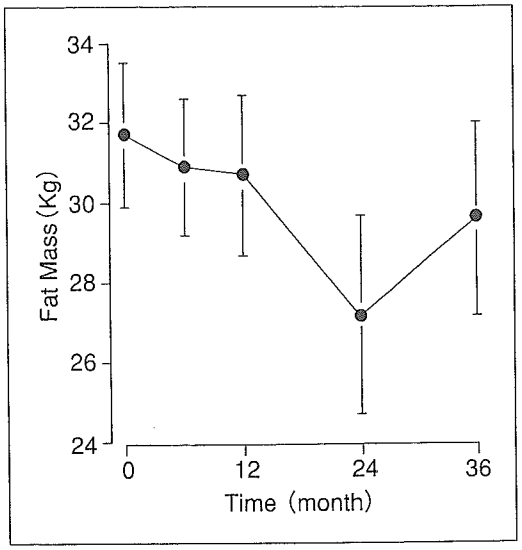

図2　性腺機能不全患者(n=16)にテストステロン補充療法を36カ月行った際の脂肪量変化(文献2より引用)

には，体脂肪率の増加と安静時エネルギー消費量の低下が認められている(図3)[3]．

これらの事実は，内因性のテストステロンはヒトにおいて，エネルギー消費を高め，体脂肪を減らす方向に作用している可能性を示唆する．実際，*in vitro* では，アンドロゲンは脂肪分解を促進する方向に作用していることが示されている．また，ゴナドトロピン放出ホルモンアンタゴニストの投与によって内因性のテストステロンを低下させた際には，脂肪組織由来のインスリン抵抗性改善作用物質として，最近注目されている血中 adiponectin 濃度が上昇し，同時に外因性のテストステロンの補充を行った場合には，その上昇が抑制されること，また外因性にテストステロンを単独で投与した際にも，血中 adiponectin 濃度が低下することが報告されている[4]．

アンドロゲン受容体遺伝子はX染色体上に存在し，ヒトではその異常は睾丸性女性化症を引き起こす．米国の Chang[5] ならびに本邦の Sato[6] のグループが，それぞれ独立にアンドロゲン受容体(AR)ノックアウトマウス(ARKOマウス)の作製に成功した．このマウスでは睾丸性女性化症の表現型が再現されると同時に，骨粗鬆症や肥満が引き起こされることが明らかにされた．ARKOのオスマウスでは，晩発性に

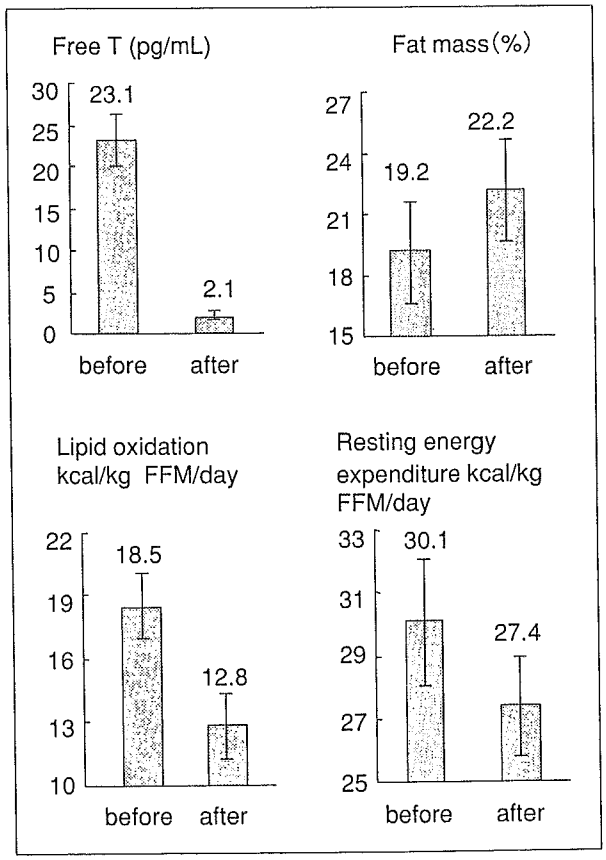

図3　健康若年男子においてGnRH製剤10週投与により性腺機能低下を引き起こした際の各種指標の変化(文献3より引用改変)
FFM：fat-free mass

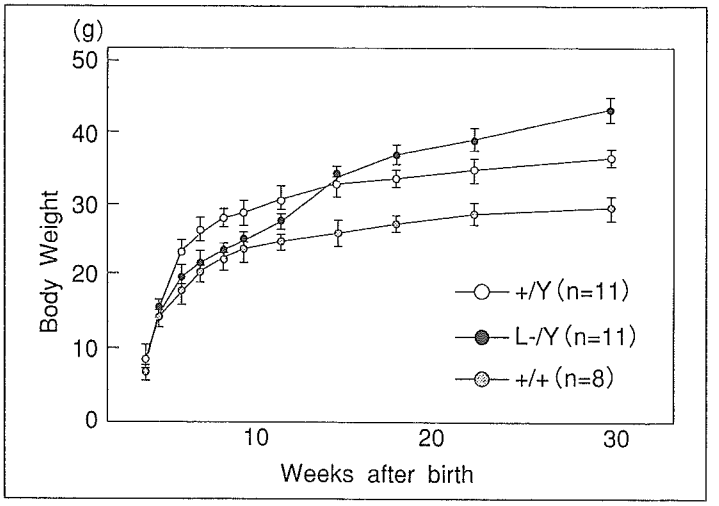

図4　アンドロゲン受容体 KO マウス(L-/Y)の体重変化
(文献 6 より引用)
+/Y：オス野生型
L-/Y：オスアンドロゲン受容体 KO マウス
+/+ ：メス野生型
オスアンドロゲン受容体 KO マウスでは晩発性の体重増加を認める.

皮下および腹部内臓周囲の白色脂肪組織の増加と肥満を来すことが明らかになった(図4)[6].

このような現象はメスの ARKO マウスでは観察されず，オスに特有の現象と考えられた．ヒトにおける AR の遺伝的異常で引き起こされる睾丸性女性化症では，血中テストステロン値は正常もしくは高値となるが，本マウスでは，高度の精巣委縮のためにテストステロン値は低下していた．基質であるテストステロンの低下のためにアロマターゼ活性を介したエストロゲンの産生が低い可能性が考えられるが，実際には本マウスの血中 E2 濃度は正常であり，肥満は少なくとも低エストロゲン血症によって引き起こされたものではないと考えられた．

われわれは肥満機序を野生型オスマウスとの比較において検討した結果，ARKO オスマウスでは自発運動量と酸素消費量の低下を認めた．酸素消費量低下の一因として，ARKO マウスでは白色脂肪組織の熱産生蛋白の UCP-1 の発現低下が一因と考えられた，また，白色脂肪では後述の aromatase KO マウスの場合[7]と異なり，脂肪分解系酵素の発現低下を認め，同じ肥満でも WAT 性状の違いが示唆された．

以上より，ARKO マウスの肥満の成因にはエネルギー消費の低下と脂肪分解系酵素の低下が関与すると考えられた．一方，肥満を呈しながら本マウスの耐糖能ならびにインスリン感受性は正常であったが，その原因としてインスリン感受性促進効果をもつ血中 adiponectin 濃度の高値が一因と考えられた[8]．Nishizawa ら[9]は，テストステロンは脂肪細胞よりの adiponectin 分泌を抑制することを報告しており，本マウスの血中 adiponectin 濃度の上昇を説明するものと考えられる．これらのデータは，ヒト男性における既述のテストステロンの adiponectin 分泌低下作用をよく説明する．内因性テストステロンは，インスリン抵抗性に関しては増悪の方向に作用する可能性ある[8].

エストロゲン

エストロゲンの最終合成酵素である Cytochrome P450 aromatase の欠損症例やエストロゲン受容体(estrogen receptor：ER) α の欠損症例が発見されて以来，内因性エストロゲンと脂肪蓄積，糖質・脂質代謝，インスリン感受

性などとの関連が少しずつ明らかにされつつある．Aromatase 欠損症の患者では躯幹部中心の脂肪蓄積型の肥満を呈すること，一方，ERα欠損男性患者では重症の骨粗鬆症と同時に，空腹時血糖とインスリンの上昇が報告されている[10]．

ERαKO マウスでは，食餌摂取量には野生型との間に差を認めなかったが，週齢の増加とともに4～8カ月頃に白色脂肪重量と体重の増加を認めた[11]．脂肪は肥大を来し，平均エネルギー消費量は，野生型に比べて減少していた．ERβKO マウスではこのような現象は認められず，白色脂肪増加の表現型はERαに特異的と考えられている[12]．一方，aromatase ノックアウトマウスでも，オス，メスともに摂餌量はむしろ低下しているにもかかわらず，WAT の増加と脂肪細胞の肥大により体重増加を来し，1年後には高レプチン，高コレステロール，高TG，高インスリン血症を来し，メタボリックシンドロームともいうべき病態を示した[13]．また野生型に比べて，自発運動量の低下や lean body mass の低下，ブドウ糖酸化率の低下を認めたが，安静時のエネルギー消費量には差が認められなかった．

これらの結果から，エストロゲン欠乏は身体活動の低下を介してエネルギー消費量の減少をもたらす可能性が推察される．また，aromatase ノックアウトマウスでは，脂肪分解の抑制よりはむしろ脂肪合成系の亢進が脂肪蓄積の原因と推察されている[7]．また上記2つの肥満モデルでは，インスリン抵抗性の存在が示唆されている．すなわち糖負荷試験におけるERαKO マウスの血糖は野生型に比べ高く，血清インスリン値も高値であった．Jones らは，生後1年の aromatase KO マウスでは血糖値には差がなかったものの，血中インスリン値は野生型の約4倍の高値を報告している[13]．

おわりに

内因性のエストロゲンは，インスリン感受性を増大し，体脂肪の増加を防ぐ方向に働いていると考えられる．一方，内因性のテストステロンも体脂肪の増加を防ぐ方向に作用するが，インスリン感受性は低下させる方向に作用していると考えられる（表1にテストステロンとエストロゲンの対比をまとめた）．中高年以降のいわゆる「中年太り」や生活習慣病の発症要因の一因として，加齢に伴う性ステロイドの低下が関係している可能性が考えられる．

内臓脂肪蓄積を抑制するような代謝に特化した男性ホルモン作用を有し，前立腺刺激作用を有さぬような SARM（selective androgen receptor modulator）の開発が可能になれば，今後，中高年以降の生活習慣病治療薬の1つとして有望かもしれない．

表1　内因性のテストステロンとエストロゲンの脂肪代謝に関する比較

	テストステロン	エストロゲン
脂肪蓄積（肥満）	↓	↓
脂肪合成	～	↓
脂肪分解	↑	～
インスリン抵抗性	↑	↓
adiponectin	↓	～

主に病態モデル動物における研究結果に基づく．ヒトにおける作用は，未だ必ずしも明確ではない．

文　献

1) Kyle UG et al：Age-related difference in fat-free mass, skeletal muscle, body cell mass and fat mass between 18 and 94 years. Eur J Clin Nutr 55：663-672, 2001.
2) Synder PJ et al：Effects of testosterone replacement in hypogonadal men. J Clin Endocrinol Metab 65：2670-2677, 2000.
3) Mauras N et al：Testosterone deficiency in young men：marked alterations in whole body protein kinetics, strength, and adiposity. J Clin Endocrinol Metab 83：1886-1992, 1998.
4) Page ST et al：Testosterone administration suppresses adiponectin levels in men. J Androl 26：85-92, 2005.
5) Yeh S et al：Generation and characterization of androgen receptor knockout（ARKO）mice：an *in vivo* model for the study of androgen functions in selective tissues. Proc Natl Acad Sci USA

99：13498-13503, 2002.
6) Sato T et al：Late onset of obesity in male androgen receptor-deficient(AR KO)mice. Biochem. Biophys. Res Commun 300：167-171, 2003.
7) Misso M et al：Cellular and molecular characterization of the adipose phenotype of the aromatase-deficient mouse. Endocrinol 144：1474-1480, 2003.
8) Fan W et al：Androgen receptor null male mice develop late-onset obesity due to decreased energy expenditure and lypolytic activity but show normal insulin sensitivity with high adiponectin secretion. Diabetes 2005 in press.
9) Nishizawa H et al：Androgens decrease plasma adiponectin, an insulin-sensitizing adipocyte-derived protein. Diabetes 51：2734-2741, 2002.
10) 柳瀬敏彦：性腺におけるインスリン作用．内分泌・糖尿病科，2005(印刷中)．
11) Heine PA et al：Increased adipose tissue in male and female estrogen alpha knockout mice. Proc Natl Acad Sci USA 97：12729-12734, 2000.
12) Couse J F et al：Estrogen receptor null mice：what have we learned and where will they lead? Endocr Rev 20：358-417, 1999.
13) Jones MEE et al：Aromatase-deficient (ArKO) mice have a phenotype of increased adiposity. Proc Natl Acad Sci USA 97：12735-12740, 2000.

(執筆者連絡先) 柳瀬敏彦 〒812-8582 福岡県福岡市東区馬出 3-1-1 九州大学大学院医学研究院病態制御内科

Available online at www.sciencedirect.com
SCIENCE DIRECT®
Biochemical and Biophysical Research Communications 341 (2006) 192–201
BBRC
www.elsevier.com/locate/ybbrc

Identification of the functional domains of ANT-1, a novel coactivator of the androgen receptor ☆

Shuli Fan, Kiminobu Goto [1], Guangchun Chen, Hidetaka Morinaga, Masatoshi Nomura, Taijiro Okabe, Hajime Nawata, Toshihiko Yanase *

Department of Medicine and Bioregulatory Science (3rd Department of Internal Medicine), Graduate School of Medical Sciences, Kyushu University, Maidashi 3-1-1, Higashi-ku, Fukuoka 812-8582, Japan

Received 29 November 2005
Available online 9 January 2006

Abstract

Previously, we identified a transcriptional coactivator for the activation function-1 (AF-1) domain of the human androgen receptor (AR) and designated it androgen receptor N-terminal domain transactivating protein-1 (ANT-1). This coactivator, which contains multiple tetratricopeptide repeat (TPR) motifs from amino acid (aa) 294, is identical to a component of U5 small nuclear ribonucleoprotein particles and binds specifically to the AR or glucocorticoid receptor. Here, we identified four distinct functional domains. The AR-AF-1-binding domain, which bound to either aa 180–360 or 360–532 in AR-AF-1, clearly overlapped with TAU-1 and TAU-5. This domain and the subnuclear speckle formation domain in ANT-1 were assigned within the TPR motifs, while the transactivating and nuclear localization signal domains resided within the N-terminal sequence. The existence of these functional domains may further support the idea that ANT-1 can function as an AR-AF-1-specific coactivator while mediating a transcription-splicing coupling.

Keywords: Androgen receptor; Activation function-1; Nuclear localization signal; Small nuclear ribonucleoprotein particle; Splicing factor compartment; Tetratricopeptide repeat; Transcriptional coactivator

The androgen receptor (AR) harbors two transcription activation function (AF) domains: the constitutively active AF-1 located in the N-terminal transactivating domain and the ligand-dependent AF-2 within the C-terminal ligand-binding domain [1]. The AR is considered to be quite unique among the members of the nuclear receptor superfamily, because most, if not all, of its activities are mediated via the ligand-independent constitutive activity of AF-1 [2,3]. This is in strong contrast to estrogen receptor α (ER α), in which the overall transactivation capacities are primarily dependent on AF-2 [4]. The AR shares hormone response element sequences on the DNA with the receptors for glucocorticoids (GR), mineralocorticoids, and progesterone [5]. In this regard, the N-terminal domain (NTD), which varies among these receptors, is thought to be responsible for the cell- and ligand-specific regulation of their target genes [6]. The fundamental role of AR-AF-1 was further supported by our clinical finding that the absence of an AR-AF-1-specific transcription coactivator results in androgen insensitivity syndrome [7]. To date, in addition to p300/CBP, SRC-1 and caveolin-1, which interact with both AF-1 and AF-2 [2,8,9], almost 20 proteins have been proposed to bind to the AR N-terminal transactivating domain, including basal transcription factors such as TFIIF [10], co-repressors [11–13], and

☆ *Abbreviations:* aa, amino acid(s); AF, activation function; ANT-1, androgen receptor N-terminal domain-binding protein-1; AR, androgen receptor; DHT, dihydrotestosterone; ER, estrogen receptor; GR, glucocorticoid receptor; NLS, nuclear localization signal; NTD, N-terminal domain; SFC, splicing factor compartment; snRNP, small nuclear ribonucleoprotein particle; TPR, tetratricopeptide repeat.

* Corresponding author. Fax: +81 92 642 5297.
E-mail address: yanase@intmed3.med.kyushu-u.ac.jp (T. Yanase).
[1] Present address: Internal Medicine and the Elderly Care, Kasamatsukai Medical Corporation Ariyoshi Hospital, Oo-aza Kamiariki 397-1, Miyata, Kurate-gun County, Fukuoka 823-0015, Japan.

0006-291X/$ - see front matter © 2005 Elsevier Inc. All rights reserved.
doi:10.1016/j.bbrc.2005.12.167

coactivators [14,15] as well as other unique proteins, including cyclin E [16], breast cancer susceptibility gene 1 (*BRCA1*) [17], and the RNA molecule SRA [18].

We previously isolated a cDNA sequence encoding a novel coactivator for the AR [19]. This protein, designated AR NTD transactivating protein-1 (ANT-1), bound to the AF-1 of the AR and GR, but not that of ER α, and specifically enhanced the AR- and GR-AF-1 transactivation capacities in a ligand-independent manner. The amino acid sequence of ANT-1 was identical to that of the PRP6 protein [20,21], a mammalian homolog of yeast prp6p, which forms U5 small nuclear ribonucleoprotein particles (snRNPs) involved in the spliceosome. In addition to ANT-1, cyclin E [22] and $p54^{nrb}$ [23], another AR-AF-1-binding protein, are also known to interact with splicing factors, suggesting that AR-AF-1 may be involved in the pre-mRNA splicing machinery. Upon confocal microscopic image analysis, ANT-1 was compartmentalized into 20–40 coarse splicing factor compartment (SFC) speckles against a background of diffuse reticular distribution [19]. Interestingly, the ANT-1 sequence shows structural significance, since it contains 19 copies of the tetratricopeptide repeat (TPR) motif, which plays significant roles in protein–protein interactions [24], in the final two-thirds of the C-terminal region.

It has been hypothesized that active gene transcription may occur simultaneously with pre-mRNA processing, and this process has been designated co-transcriptional splicing or "transcription-splicing coupling" [25,26]. Furthermore, steroid hormones affect the processing of pre-mRNA synthesized from steroid-sensitive promoters, but not from steroid-unresponsive promoters [27]. The nucleus contains different sets of functional compartments, often called "speckles," which include SFCs showing nearly 20–50 large speckles [28]. After three-dimensional reconstruction of confocal microscopic images, we observed that the activated AR forms 200–400 fine speckles that chiefly recruit AF-2-interacting transcriptional cofactors [29,30]. These speckles are mostly located in euchromatin regions and merge with the diffuse distribution of ANT-1. In contrast to cytoplasmic compartments, the subnuclear compartments are not sequestered by membrane structures, thereby allowing rapid movement of the protein components across the compartment. Therefore, interaction of ANT-1 with the AR or GR in the diffuse distribution of ANT-1 may play a role in the interaction between these two distinct subnuclear compartments. We speculated that it should contain at least four functional domains, namely a nuclear localization signal (NLS) domain, a transactivating domain, a speckle formation domain, and an AR-AF-1-binding domain. Therefore, in the present study, we performed analyses to investigate the presence of these functional domains in ANT-1.

Materials and methods

Cell culture. COS-7 cells and NIH3T3 fibroblast cells were maintained in Dulbecco's modified Eagle's medium supplemented with 10% fetal calf serum. To establish cells (designated COS-AR-AF-1 cells) that stably expressed AR-AF-1 (amino acids (aa) 1–532), COS-7 cells in 10 cm dishes were transfected with 5 μg of an AR-AF-1 expression plasmid [7] using the Superfect Transfection Reagent (Qiagen) according to the manufacturer's instructions. An initial selection was performed with 1 μg/ml of puromycin (Sigma) at 24 h after the transfection, and the selected cells were subsequently grown in bulk culture for 5–6 days. A single clone was isolated by limited dilution and then cultured for a further 2 weeks. The presence of the AR-AF-1 fragment in the stably transfected line was monitored by Western blotting using an anti-AR N-20 antibody (Santa Cruz Biotechnology).

Plasmids and site-directed mutagenesis. pMMTV-luc, containing the luciferase gene driven by the mouse mammary tumor virus long terminal repeat harboring a hormone response element for both the AR and GR, and the plasmids expressing ANT-N and ANT-C were described previously [7,19]. The expression plasmid for human ER α (pSG5-ER α) and a reporter plasmid for ER α (pERE2-tk109-luc) were provided by Dr. Shigeaki Kato (University of Tokyo, Tokyo, Japan). pANT-1-myc expressing myc-tagged full-length ANT-1 was prepared as described previously [19], and plasmids expressing truncated mutants of myc-tagged ANT-1 were obtained by appropriate restriction enzyme digestion or PCR amplification. Briefly, ΔANT(290) was obtained by restriction digestion with *Kpn*I and *Eco*RV. For ΔANT(146), ΔANT(172), ΔANT(399), ΔANT(499), and ΔANT(173–499) PCR was initially performed to create DNA fragments that contained a *Kpn*I restriction site at the 5′ end and an *Xba*I restriction site at the 3′ end. These fragments were then digested with *Kpn*I and *Xba*I, and subcloned into appropriate expression plasmids such as pcDNA3, pcDNA3-myc-his or pEGFP.

We used the Check Mate Mammalian Two-Hybrid System (Promega), in which the GAL-4 DNA-binding domain is present in a pBind plasmid, the herpes simplex virus VP16 activation domain is present in a pACT plasmid, and five GAL-4-binding sequences and a luciferase gene are present in the pG5luc plasmid. Truncated fragments of ANT-1 with an *Xba*I restriction site at the 5′ end and a *Kpn*I site at the 3′ end were obtained by PCR amplification and then subcloned into pACT to generate VP-ΔANT(146), VP-ΔANT(172), VP-ΔANT(290), VP-ΔANT(399), VP-ΔANT(499), and VP-ANT-C. Truncated fragments of the AR-NTD with a *Bam*HI restriction site at the 5′ end and an *Xba*I site at the 3′ end were also obtained by PCR amplification and then subcloned into pBind plasmids to generate GAL-AR(1–180), GAL-AR(180–360), GAL-AR(360–520), and GAL-AR(1–660).

Site-directed mutagenesis was performed using a Quick Change Site-directed Mutagenesis Kit (Stratagene) according to the manufacturer's protocols. The pEGFP plasmid harboring the ΔANT(172) sequence was used as a template.

Transient transfection and mammalian two-hybrid assays. COS-7 cells (5×10^5 cells per well in six-well plates) were transiently transfected using a Superfect Transfection Kit (Qiagen). Generally, 2.5 μg of plasmid DNA per well (0.2–1.0 μg of pcDNA3-ANT-1-deletion mutants, 0.2 μg of pCMVhAR [7], and 1.0 μg of pMMTV-luc) was used for the transfection, and the total amount of transfected DNA was kept constant by adding the pcDNA3 plasmid. At 16 h post-transfection, the cells were rinsed in PBS and then cultured in medium containing 10% charcoal-stripped fetal calf serum with or without a steroid hormone (10^{-8} M dihydrotestosterone (DHT)) for an additional 18 h. Subsequently, the cells were harvested and assayed for their luciferase activities using the Dual-Luciferase Reporter Assay System (Promega).

For mammalian two-hybrid assays, NIH3T3 cells were used according to the recommendations included in the Check Mate Mammalian Two-Hybrid System. At 24 h after plating at 10^5 cells per well in 12-well plates, the cells were transiently transfected with 500 ng of pG5luc, 100 ng of VP16 plasmids, and 300 ng of GAL4 plasmids. At 24 h post-transfection, luciferase assays were performed as described above.

Immunoprecipitation. Either COS-AR-AF-1 or COS-7 cells were subjected to transient transfection. Immunoprecipitation was performed as previously described [19]. Briefly, at 24 h post-transfection, whole cell lysates were prepared by lysing the cells in lysis buffer (1.0% Nonidet P-40, 50 mM Tris–HCl, pH 7.8, 150 mM NaCl, 1 mM DTT, and 1 tablet of

protease inhibitor mixture/10 ml buffer). After pre-clearing with protein G–Sepharose beads (Pharmacia), the lysates were incubated with an antibody against c-myc (Santa Cruz Biotechnology) for truncated ANT-1 or an antibody against the NTD of AR N-20 for the truncated ARs in immunoprecipitation (IP) buffer (1.0% Nonidet P-40, 50 mM Tris–HCl, pH 7.8, 200 mM NaCl, 1 mM DTT, and 1 tablet of protease inhibitor mixture/10 ml buffer) at 4 °C for 1 h, and then further incubated with protein G–Sepharose beads at 4 °C for 2 h. The immunoprecipitates were subsequently analyzed by Western blotting using antibodies against AR N-20 or c-myc.

Microscopy and imaging analysis. The cells were divided into 35-mm glass-bottomed dishes (MatTek Corporation) and then transfected with 0.5 μg of the plasmids using 2.5 μl Superfect reagent/dish. At 6–18 h post-transfection, the culture medium was replaced with fresh DMEM. The cells were first imaged without any hormone treatment and then incubated with 10^{-8} M DHT for 1 h. After the incubation, the cells were imaged again using a confocal laser scanning microscope (Leica TCS-SP system; Leica Microsystems). The green fluorescence in the cells was excited using the 488 nm line from an argon laser and the emission was viewed through a 500–550 nm band pass filter.

Results

Activation function and subcellular localizations of ANT-1 deletion mutants

In a previous paper, we demonstrated that an ANT-1 deletion mutant comprised of aa 78–495 (designated ANT-N) showed nearly full enhancement (about 90%) of the ligand-independent AR-AF-1 transactivation capacity of full-length ANT-1, while a deletion mutant comprised of aa 496 to the C-terminus of ANT-1 (designated ANT-C) did not show any enhancement [19]. Therefore, in the present study, ΔANT(499) covering the N-terminal half of ANT-1 was serially deleted from the C-terminal end to generate ΔANT(399), ΔANT(290), ΔANT(172), and ΔANT(146), respectively, in addition to ΔANT(173–499) (Fig. 1A). These fragments were then subcloned into appropriate plasmids to generate plasmids expressing the ANT-1 deletion mutants with and without fusion to GFP. As previously shown, full-length ANT-1 enhanced the transactivation function of the AR, which is activated in the presence of 10^{-8} M DHT, by inducing nearly four-fold enhancement of the AF-1 function. ΔANT(499), ΔANT(399), ΔANT(290), and ΔANT(172) each enhanced the AR-dependent transactivation by about 90% of the level induced by full-length ANT-1, indicating that aa 78–172 are important for the transactivation induced by ANT-1 (Fig. 1B). In contrast, when aa 147–172 were deleted (ΔANT(146)), the transactivation function was almost negligible. This result was further confirmed by the findings that neither ΔANT(173–499) nor ANT-C were able to induce any transactivation.

Next, we investigated the subcellular and intranuclear distributions of the ANT-1 deletion mutants fused in-frame to GFP. Representative confocal microscopic images of COS-7 cells transfected with the expression plasmids for the fusion proteins are shown in Fig. 2. As previously demonstrated, full-length ANT-1-GFP showed two distinct distributions in the nucleus: a diffuse reticular distribution

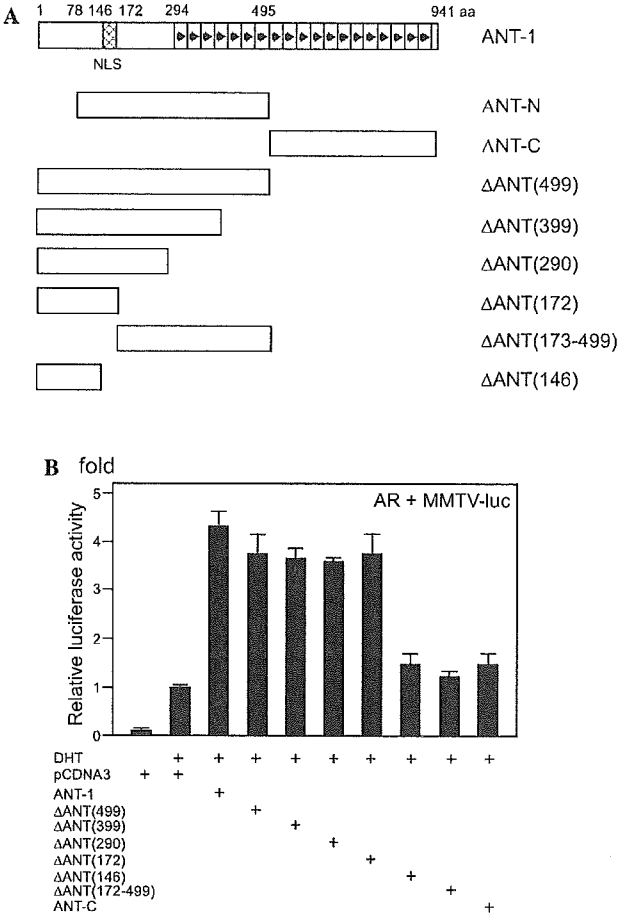

Fig. 1. Schematic diagrams of the human ANT-1 deletion mutants and their transactivation functions. (A) Schematic diagrams of the ANT-1 truncated mutants used in the experiments. The structure of full-length ANT-1 is shown at the top. ANT-1, a binding protein for U5 snRNP, consists of 941 aa and possesses 19 TPR motifs from aa 294 within the last two-thirds of the C-terminal region (shown by arrowheads in open boxes). The putative NLS is shown as a hatched box. ANT-N (aa 78–495) and ANT-C (aa 495–941) were reported previously. All the truncated fragments were subcloned into appropriate plasmids and subjected to reporter assays, confocal microscopic observation, mammalian two-hybrid assays, and immunoprecipitation. (B) Transactivation functions of the truncated mutants of ANT-1. COS-7 cells were transfected with the empty pcDNA3 plasmid (pcDNA3) or pcDNA3 harboring full-length ANT-1 or its deletion mutants (ΔANT(499) to ANT-C), a plasmid expressing the full-length AR (molar ratio 5:1) and a pMMTV-luc reporter plasmid, and then treated with 10^{-8} M DHT. The relative enhancement of the luciferase activity compared with that after co-transfection with the empty pcDNA3 plasmid in the presence of 10^{-8} M DHT is expressed as the -fold induction.

throughout the nucleus and 20–40 coarse subnuclear speckles (Fig. 2A) [19]. ΔANT(499)-GFP and ΔANT(399)-GFP showed similar distributions in the nucleus to the full-length fusion protein (Figs. 2B and C). In contrast, ΔANT(290)-GFP, which lacked aa 290–399, did not form any subnuclear speckles and showed only a diffuse distribution in the nucleus (compare Figs. 2C and D), while retaining the transactivation function on the AR (Fig. 1B). These results suggest that the region required for ANT-1 to

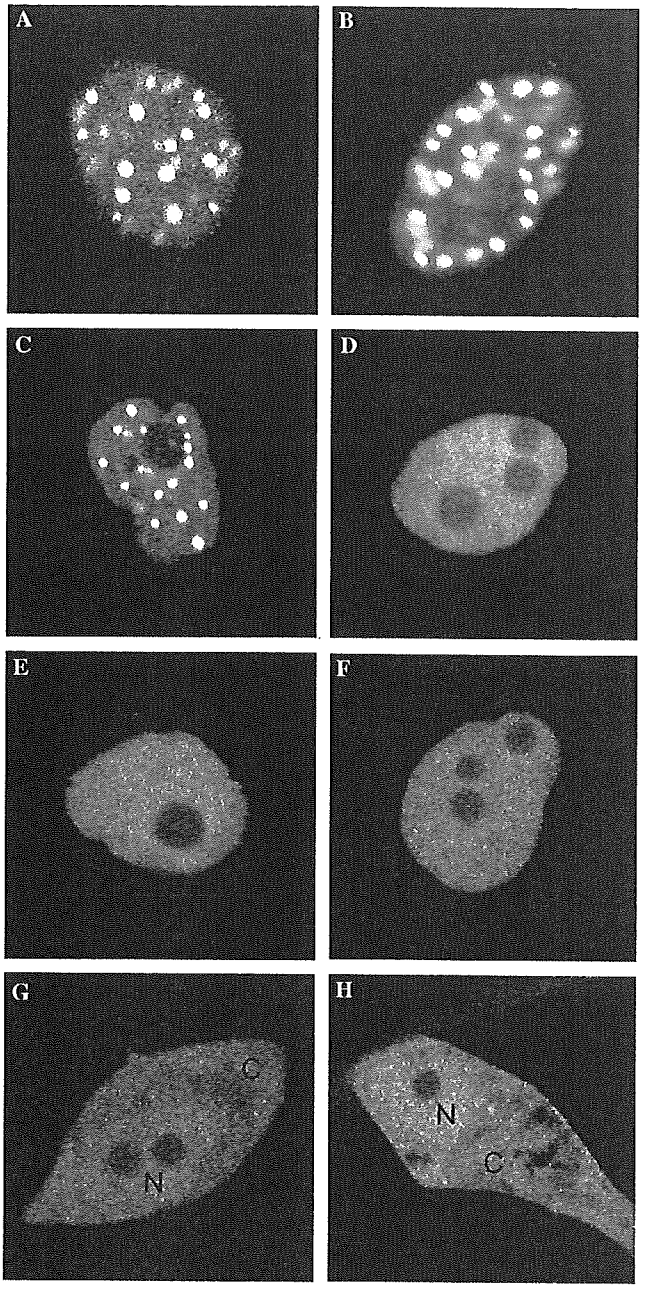

Fig. 2. Confocal microscopic images of the full-length and truncated mutants of ANT-1 fused to GFP. (A–H) COS-7 cells were transiently transfected with pEGFP harboring full-length ANT-1 (A) or its truncated mutants (B–H) and then observed by confocal microscopy. (B) ΔANT(499); (C) ΔANT(399); (D) ΔANT(290); (E) ΔANT(200); (F) ΔANT(172); (G) ΔANT(146); (H) ΔANT(173–499). In addition to the ANT-1 deletion mutants shown in Fig. 1A, a deletion mutant of ANT-1 comprising aa 1–200 (E) was used in the experiments. In (A–F) only the nucleus shows fluorescence. In (G,H) N, nucleus; C, cytoplasm.

generate intranuclear speckles is located between aa 291 and 399, and that speckle formation is not required for the transactivation function of ANT-1. Furthermore, ΔANT(146)-GFP and ΔANT(173–499)-GFP were not concentrated in the nucleus, but diffusely distributed throughout both the nucleus and the cytoplasm, suggesting that the 26 aa sequence from aa 146 to 172 confers nuclear localization (compare Figs. 2F and G).

The NLS and receptor-specific transactivation capacity of ANT-1

The region from aa 145 to 172 contains bipartite basic amino acid stretches, often found in an NLS, separated by a 20 aa interval, namely Lys(146)-Arg(147)-Lys(148) and Lys(169)-Arg(170)-Arg(172). Thus, using the plasmid expressing ΔANT(172)-GFP as a template, we performed site-directed mutagenesis to mutate these basic amino acids in the first stretch alone (ΔANT(172)M1), the second stretch alone (ΔANT(172)M2 and M3), and both stretches (ANT(172)M4 and M5) (Fig. 3A). The mutated plasmids were then transfected into COS-7 cells and observed by confocal microscopy (Fig. 3B). ΔANT(172)M1, ΔANT(172)M2, and ΔANT(172)M3 all showed partial disruption of the nuclear concentration of the fluorescence (panels b–d), thereby generating cytoplasmic fluorescence. When both the first and second stretches were simultaneously mutated, the nuclear translocation of the fusion proteins (ΔANT(172)M4 and ΔANT(172)M5) was almost completely disrupted and resembled that of ΔANT(146) (panels e and f), indicating that these bipartite basic amino acid stretches are the NLS of ANT-1.

When the transactivation capacities of these ΔANT(172) mutants were compared with that of wild-type ΔANT(172), we found that the transactivation function of each mutated fragment was almost completely abolished. As shown in Fig. 3C, even when the nuclear fluorescence was partially disturbed but still much stronger than that in the cytoplasm, the ΔANT(172)M1, ΔANT(172)M2, and ΔANT(172)M3 mutants still did not enhance AR-dependent transactivation. These results indicate that the basic amino acids within this 27 aa sequence may play roles in both the nuclear translocation and the transactivation function of ANT-1.

To test the receptor specificity of the transactivation domain of ANT-1 contained in ΔANT(172), a plasmid expressing ΔANT(172) was transiently transfected into COS-7 cells with an expression plasmid for the AR, GR or ER α. As shown in Fig. 4, co-expression of ΔANT(172) specifically enhanced either the AR or GR, but not ER α, in a dose-dependent manner until the molar ratio of ANT-1:AR was 4:1. When the quantity of the ANT-1 expression plasmid was extremely high (10:1), the TK-driven promoter harboring the estrogen response element or the TK promoter itself was enhanced by twofold. Under these experimental conditions, the AR- or GR-dependent transactivation system was enhanced by 12- to 15-fold. Overall, these results suggest that ΔANT(172) primarily represents the receptor specificity of ANT-1.

ANT-1 binds to AR-AF-1 through TPR motifs

We first performed mammalian two-hybrid assays using AR-AF-1 and ANT-1 deletion mutants. Possibly because

A

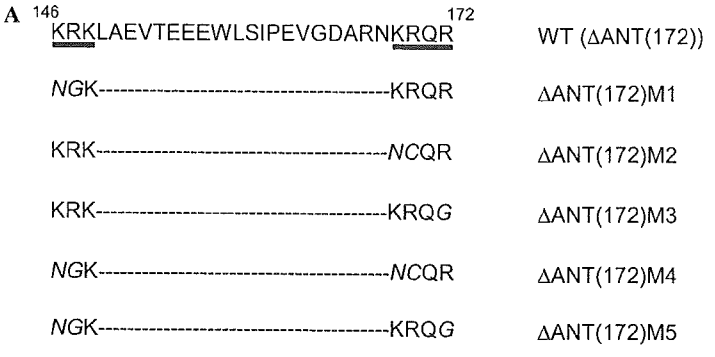
146
KRKLAEVTEEEWLSIPEVGDARNKRQR
172
WT (ΔANT(172))
NGK----------KRQR
ΔANT(172)M1
KRK----------NCQR
ΔANT(172)M2
KRK----------KRQG
ΔANT(172)M3
NGK----------NCQR
ΔANT(172)M4
NGK----------KRQG
ΔANT(172)M5

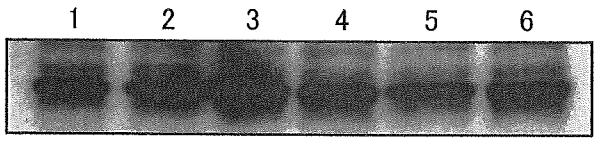
1
2
3
4
5
6

B

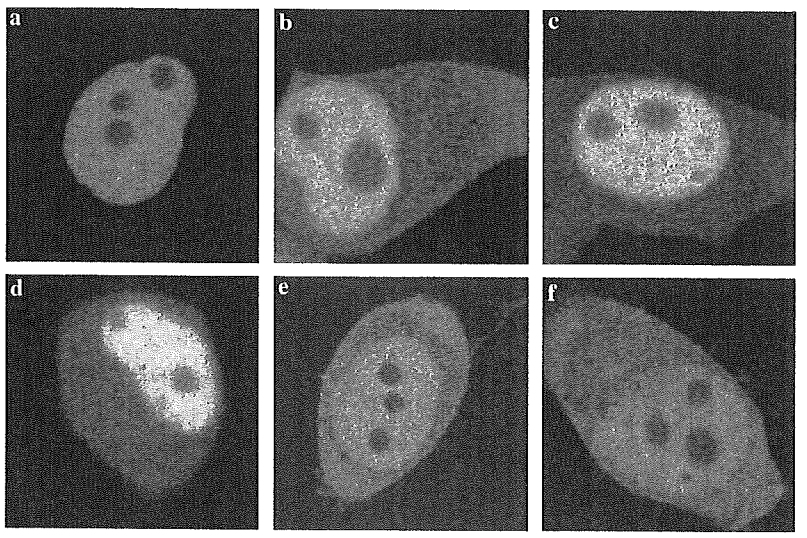
a
b
c
d
e
f

C

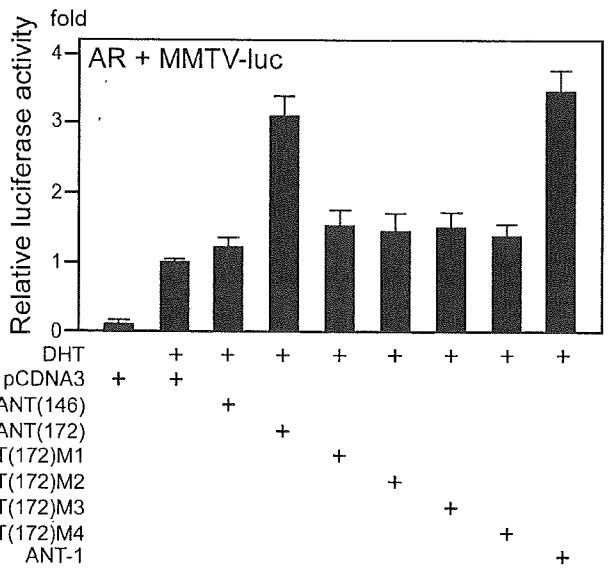
fold
Relative luciferase activity
AR + MMTV-luc
0
1
2
3
4
DHT + + + + + + + + +
pCDNA3 + +
ΔANT(146) +
ΔANT(172) +
ΔANT(172)M1 +
ΔANT(172)M2 +
ΔANT(172)M3 +
ΔANT(172)M4 +
ANT-1 +

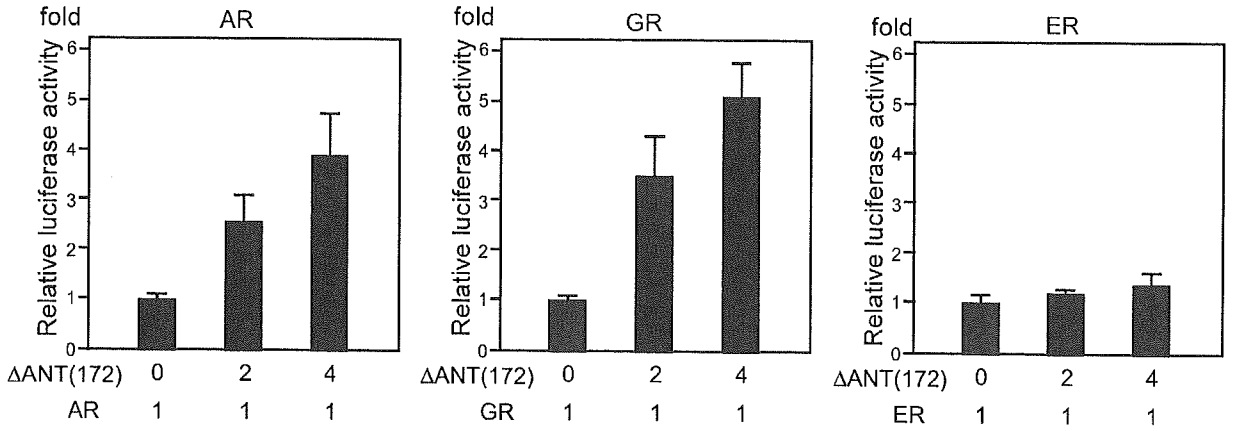

Fig. 4. Receptor-specific transactivation of ΔANT(172). An expression plasmid for ΔANT(172) was transiently transfected into COS-7 cells with expression plasmids for the AR, GR or ER α, together with appropriate reporter plasmids (pMMTV-luc for the AR or GR, and pERE2-tk109-luc for ER α), and then treated with steroid hormones (10^{-8} M DHT, 10^{-7} M dexamethasone or 10^{-8} M estradiol). Co-transfection of the plasmid expressing ΔANT(172) shows specific enhancement of the AR and GR, but not ER α, in a dose-dependent manner until the molar ratio of ANT-1 to the AR or GR reaches 4:1.

AR-AF-1 possesses strong autonomous transactivation capacity, transfection of NIH3T3 cells with the empty VP16 plasmid without any insertion conferred background luciferase activity driven by the GAL-4-containing AR-AF-1 (ΔAR(660)). Therefore, the background activity exerted by the presence of GAL-ΔAR(660) and the VP16 plasmid without an insertion was set as the standard and compared to the activities induced with the VP16 plasmids containing the ANT-1 deletion mutants (Fig. 5). Insertion of full-length ANT-1 into the VP16 plasmid (VP-ANT) or ΔANT(499) truncated in the seventh TPR of the 19 TPR repeats (Fig. 1A) strongly increased the luciferase activities by fivefold. When the sequence from aa 399 (in the fourth TPR) to 499 was deleted, the luciferase activity was weakly increased by twofold. The VP16 plasmid harboring ANT-C, containing 12.5 TPR motifs located at the C-terminal side, also showed about a 2.5-fold increase in the luciferase activity.

Next, we performed immunoprecipitation experiments using lysates of COS-7 cells stably expressing AR-AF-1 (COS-AR-AF-1 cells) transfected with plasmids expressing the ANT-1 deletion mutants tagged with myc. As shown in Fig. 6, only full-length ANT-1 and ΔANT(499) were co-immunoprecipitated with AR-AF-1 (lanes 1 and 2), whereas the other deletion mutants, including ΔANT(399) and ANT-C, were not. Taken together, these results indicate that ANT-1 binds to AR-AF-1 primarily via aa 399–499, encompassing the region from the fourth to the seventh TPR motifs.

ANT-1 binds to the AR sequence between either aa 180–360 or aa 360–532 within AF-1

We created plasmids expressing the AR-AF-1 region divided into three smaller fragments, namely aa 1–180, aa 180–360, and aa 360–532, and performed mammalian two-hybrid assays using ΔAR(660) containing the whole NTD and the DNA-binding domain (DBD) as a control (Fig. 7A). The results revealed that both ΔAR(180–360) and ΔAR(360–532) bound to ΔANT(499), whereas ΔAR(180) did not. Furthermore, the binding was confirmed by immunoprecipitation experiments (Fig. 8). ΔANT(499) was co-immunoprecipitated with either ΔAR(180–360) or ΔAR(360–532) tagged with GAL.

Discussion

We have identified four distinct functional domains in the ANT-1 molecule, which enhances AR-AF-1 transactivation capacity. The four regions were: (1) an NLS

Fig. 3. The nuclear localization signal of ANT-1. (A) Wild-type (WT) and mutant (M1–M5) aa sequences generated by site-directed mutagenesis of ΔANT(172) for expression in COS-7 cells by transient transfection of expression plasmids. Only aa 146–172 are shown. In the WT sequence, the bipartite basic amino acid stretches are underlined. In the sequences of M1–M5, the mutated residue(s) are shown in italics. The lower panel shows the expressions of GFP fusion proteins of WT ΔANT(172) and its mutants in COS-7 cells. Western blot was performed using anti-GFP antibody. Lane 1, WT ΔANT(172); lane 2, ΔANT(172)M1; lane 3, ΔANT(172)M2; lane 4, ΔANT(172)M3; lane 5, ΔANT(172)M4; lane 6, ΔANT(172)M5. (B) Confocal microscopic images of GFP fusion proteins of WT ΔANT(172) and its mutants. COS-7 cells were transiently transfected with plasmids expressing the WT and mutant ΔANT(172)-GFP fusion proteins and then observed by confocal microscopy. (a) WT ΔANT(172); (b) ΔANT(172)M1; (c) ΔANT(172)M2; (d) ΔANT(172)M3; (e) ΔANT(172)M4; (f) ΔANT(172)M5. Mutants M1, M2, and M3 show partial disruption of the nuclear GFP fluorescence, while mutants M4 and M5 show almost complete disruption. (C) Transactivation capacities of WT and mutated ΔANT(172). The cDNA fragments expressing the mutated ΔANT(172)-GFP fusion proteins (M1–M5) were subcloned into pcDNA3 to create expression plasmids for this experiment. COS-7 cells were transfected with the empty pcDNA3 plasmid (pcDNA3) or pcDNA3 expressing the WT or mutated ΔANT(172), or WT ΔANT(146) as a control, together with a plasmid expressing the full-length AR (molar ratio 5:1) and a pMMTV-luc reporter plasmid, and then treated with 10^{-8} M DHT. The relative enhancement of the luciferase activity compared with that after co-transfection with the empty pcDNA3 plasmid in the presence of 10^{-8} M DHT is expressed as the -fold induction.

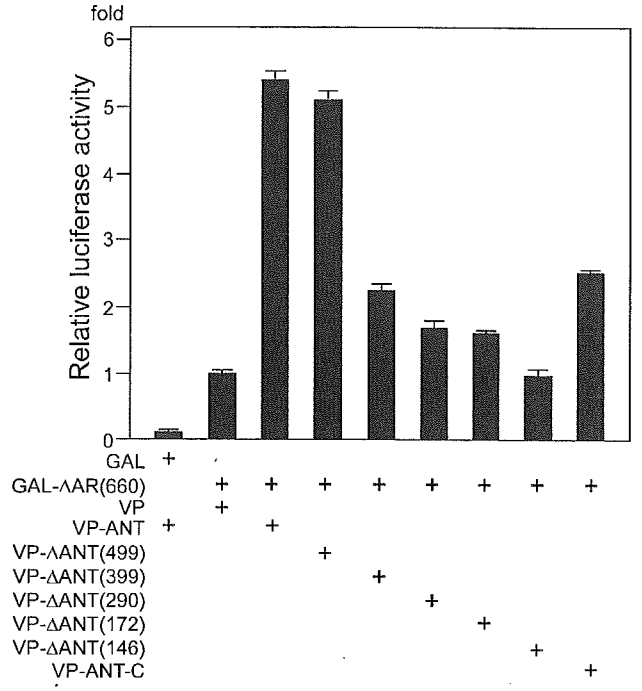

Fig. 5. Mammalian two-hybrid analysis to determine the domain within ANT-1 that binds to AR-AF-1. NIH3T3 cells were transiently transfected with 500 ng of pG5luc, 100 ng of VP16 plasmids containing full-length ANT-1 (VP-ANT) or ANT-1 truncated sequences (see Fig. 1A), and 300 ng of a GAL4 plasmid expressing aa 1–660 of the AR (see Fig. 7A) fused to GAL4. The background activity exerted by the presence of GAL-ΔAR(660) and the VP16 plasmid without an insertion was set as the standard for comparisons with the activities obtained with the VP16 plasmids containing the ANT-1 deletion mutants, and the data are presented as relative activities.

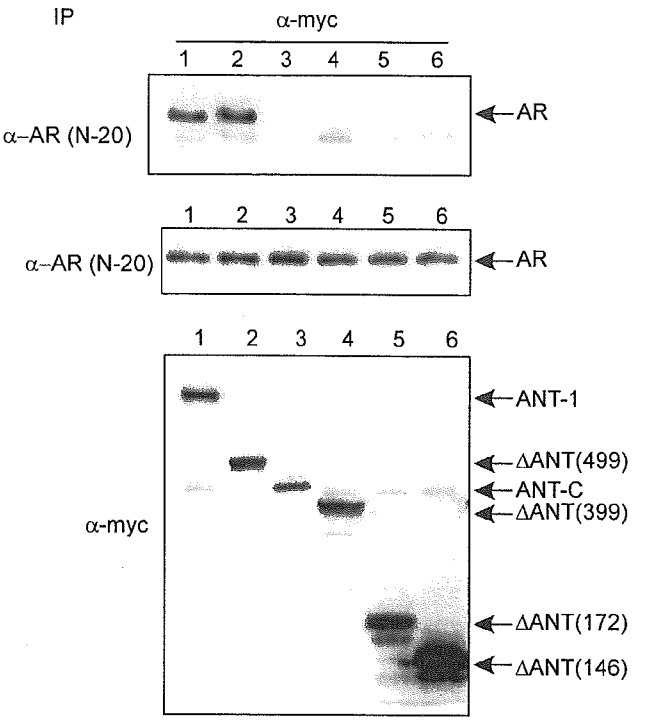

Fig. 6. Immunocoprecipitation of truncated ANT-1 mutants with AR-AF-1. COS-7 cells stably expressing AR-AF-1 (COS-7-AR-AF-1 cells) were transfected with plasmids expressing full-length or truncated mutants of ANT-1 tagged with myc. Immunoprecipitation (IP) was performed using an anti-myc antibody, and the precipitates were analyzed by Western blotting using an antibody against N-20 in AR-AF-1. The middle and bottom panels show the findings for the whole lysates used for the IP as controls. Lanes 1, full-length ANT-1; lanes 2, ΔANT(499); lanes 3, ANT-C; lanes 4, ΔANT(399); lanes 5, ΔANT(172); lanes 6, ΔANT(146).

domain; (2) a receptor-specific AF-1 transactivating domain; (3) an AR-AF-1-binding domain; (4) an intranuclear speckle formation domain. Both the NLS and ANT-1 transactivation domains were within the first 172 aa of the N-terminal region. Furthermore, the NLS of ANT-1 was tightly related to or closely overlapped with the sequence required for the transactivation function of ANT-1. Mutational analysis of the ANT-1 NLS revealed that the transactivation capacities of the intranuclear ANT-1 mutants were almost completely abolished after partial disruption of the nuclear translocation by mutations in either the first or second basic amino acid clusters. Another example of a tight relationship between a bipartite NLS and a transactivation function has been reported for the murine transcription factor distal-less (Dlx) 3, which is involved in the development and differentiation of epithelial tissue [31]. In the Dlx3 protein, the NLS sequences are part of the homeodomain sequence, and thus mutation of the NLS disrupts the sequence required for specific DNA binding, the transactivation potential, and protein–protein interactions [32]. The mechanisms for how the ANT-1 NLS confers the transactivation capacity still remain to be elucidated.

In contrast, the other two domains, required for either binding to AR-AF-1 or intranuclear speckle formation, were present within the first 7 of the 19 TPR motifs found in the ANT-1 molecule. The TPR is a structural motif present in a wide range of proteins and mediates protein–protein interactions for the assembly of multiprotein complexes. The TPR was first identified in 1990, and its name denotes the 34 amino acids comprising the basic repeat [24]. These basic repeats are usually arrayed in a tandem fashion. To date, the TPR motif has been identified in more than 25 proteins, which play important roles in diverse biological functions, including gene transcription and pre-mRNA splicing. The TPR motif has been shown to possess biological significance, since congenital mutations within the motif result in congenital disorders, such as Leber congenital amaurosis [33] and chronic granulomatous disease [34].

ANT-1 is identical to the mammalian nucleoprotein PRP6, which binds to the human splicing factor U5 snRNP (GenBank Accession No. AF221842). During the splicing step, snRNPs play critical roles in constructing the multiprotein–RNA complex known as the spliceosome. The splicing snRNPs (U1, U2, U4/U6, and U5) associate with the pre-mRNA and then with each other in an ordered

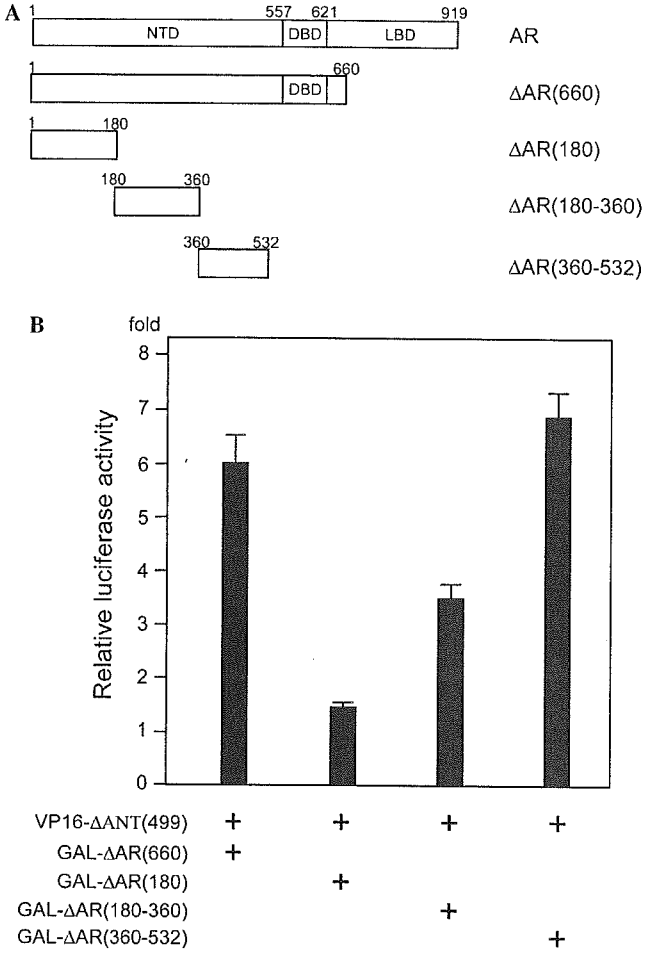

Fig. 7. Mammalian two-hybrid analysis to determine the domain within AR-AF-1 that binds to ANT-1. (A) Schematic diagrams of the truncated mutants of AR-AF-1 used for the experiment. NTD, N-terminal domain; DBD, DNA-binding domain; LBD, ligand-binding domain. (B) Mammalian two-hybrid analysis. NIH3T3 cells were transiently transfected using 500 ng of pG5luc, 100 ng of the VP16 plasmid containing ΔANT(499), or the VP16 plasmid without an insertion as a control, and 300 ng of GAL4 plasmids expressing fusion proteins with truncated mutants of the AR. In each transfection, the background activity exerted by the presence of GAL-ΔARs and the VP16 plasmid without an insertion was set as the standard for comparisons with the activities obtained with the VP16 plasmid containing ΔANT(499), and the data are expressed as the relative activities.

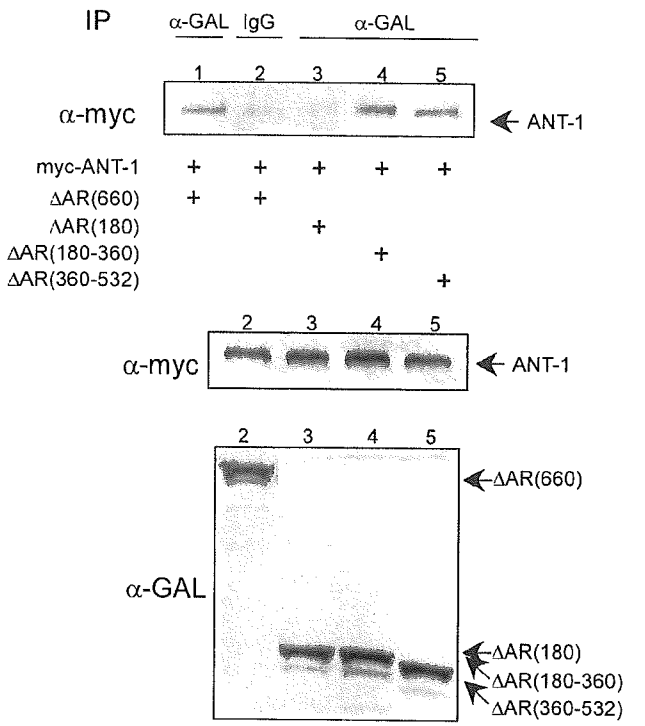

Fig. 8. Immunocoprecipitation of truncated AR mutants with ANT-1. COS-7 cells were transiently transfected with plasmids expressing truncated mutants of the AR tagged with GAL and ΔANT(499) tagged with myc. Immunoprecipitation (IP) was performed using an anti-GAL antibody for lanes 1, 3, 4, and 5 and non-immune IgG (*IgG*) for lane 2 as a control, and the precipitates were analyzed by Western blotting using an anti-myc antibody for ΔANT(499). The middle and bottom panels show the findings for the whole lysates used for the IP as controls. Lanes 1 and 2, ΔAR(660); lanes 3, ΔAR(180); lanes 4, ΔAR(180–360); lanes 5, ΔAR(360–532).

sequence to form the spliceosome, during which U5 snRNA base-pairs with exon sequences flanking the split sites. Through the sequence from aa 290 to 399 at the N-terminal end of the long TPR domain, ANT-1 may bind to the U5 snRNP multiprotein complex in the SFC, thereby forming subnuclear speckles. Although prp6p, a yeast homolog of ANT-1, was originally isolated as a spliceosomal protein, we did not observe any ANT-1-mediated enhancement of the splicing efficiency when assessed using an artificial minigene [19]. Therefore, we previously speculated that ANT-1 per se did not possess any splicing activity, but instead functioned as a transcriptional coactivator. This is in strong contrast to a spliceosomal protein SF3a p120 which is the coactivator specific for ER α-AF1 through the modulation of RNA splicing efficiency via ER α Ser118 phosphorylation [35]. In this regard, ΔANT(172), which may be unable to bind to U5 snRNP due to the absence of all the TPR motifs, showed enhancement of the AR- or GR-dependent transactivation function, but not of ER-dependent transactivation. These findings also indicated that the receptor specificity of the ANT-1-dependent transactivation function was determined by dual mechanisms: (1) via the binding specificity of ANT-1 to cognate receptors such as the AR or GR mediated by the direct binding using TPR motifs; (2) via the receptor-specific enhancement of the transactivation capacity caused by residues between aa 1 and 172, among which aa 146–172 were sufficient for the transactivation function per se. The latter receptor specificity apparently did not require the direct binding to the AR-AF-1, thus it may be exerted by another putative coactivator(s) or enhancer(s) with specific functions.

In good agreement with the subnuclear distribution of prp6p (a yeast homolog of ANT-1) [36], the intranuclear ANT-1 distribution was identical to the known distribution patterns of splicing factors [37]. Transfected ANT-1

showed two distinct distributions in the nucleus as follows: a diffuse fine reticular distribution throughout the nucleus, except for the nucleolus, and a coarsely clustered distribution (speckles) known as the SFC. In a previous paper, we speculated that the subnuclear speckle formation by ANT-1 could be independent of its transactivation function, and thus the merging of the diffuse ANT-1 distribution with the AR speckles may represent the area where ANT-1 or the ANT-1–snRNP complex meets the active AR–cofactor complex [19]. This hypothesis was supported by the current observation that the ANT-1 deletion mutants that were unable to form speckles in the nucleus retained almost the full transactivation capacity for AR-AF-1 (Figs. 1 and 2). Interestingly, mammalian PRP4K kinase (PRP4K) has been shown to be a U5 snRNP-associated kinase that interacts with BRG1, N-CoR, and mammalian PRP6 (ANT-1), and possibly phosphorylates BRG1 and PRP6 [38]. Taken together with our findings, U5 snRNP may play a role in transcription-splicing coupling.

ANT-1 bound to aa 180–360 and 360–532, respectively, within AR-AF-1. Previous studies have assigned AR-AF-1 (also called the transactivation domain or TAD) to aa 142–485 of the receptor. This region comprises both the transcription activation unit (TAU)-1 (aa 101–360) and TAU-5 (aa 360–485) domains [39,40], both of which clearly overlap with the two regions required for binding to ANT-1. Recent studies have revealed that AR-AF-1 lacks a stable secondary structure in aqueous solution, and instead is a structurally flexible polypeptide that folds into a more compact conformation in the presence of structure-stabilizing solutes [41,42]. Hence, the folding of AR-AF-1 in response to specific protein–protein interactions may create a platform for subsequent interactions in the fully competent transactivation complex. This may explain why AR-AF-1 binds many unique proteins, including a subunit of the TFIIF general transcription factor and snRNPs. In this regard, the multiple TPRs present in ANT-1 may play a role in further providing a platform for such interactions.

Acknowledgments

This study was partly supported by Grants-in-Aid for Scientific Research from the Ministry of Education, Culture, Sports, Science and Technology (to K.G. and H.N., respectively) and partly by Core Research for Evolutional Science and Technology from the Japan Science and Technology Agency (to H.N. from 1999 to 2003).

References

[1] M. Beato, S. Chavez, M. Truss, Transcriptional regulation by steroid hormones, Steroids 61 (1996) 240–251.

[2] C.L. Bevan, S. Hoare, F. Claessens, D.M. Heery, M.G. Parker, The AF1 and AF2 domains of the androgen receptor interact with distinct regions of SRC1, Mol. Cell. Biol. 19 (1999) 8383–8392.

[3] P. Alen, F. Claessens, G. Verhoeven, W. Rombauts, B. Peeters, The androgen receptor amino-terminal domain plays a key role in p160 coactivator-stimulated gene transcription, Mol. Cell. Biol. 19 (1999) 6085–6097.

[4] L. Tora, J. White, C. Brou, D. Tasset, N. Webster, E. Scheer, P. Chambon, The human estrogen receptor has two independent nonacidic transcriptional activation functions, Cell 59 (1989) 477–487.

[5] C.A. Quigley, A. De Bellis, K.B. Marschke, M.K. el-Awady, E.M. Wilson, F.S. French, Androgen receptor defects: historical, clinical, and molecular perspectives, Endocr. Rev. 16 (1995) 271–321.

[6] L. Tora, H. Gronemeyer, B. Turcotte, M.P. Gaub, P. Chambon, The N-terminal region of the chicken progesterone receptor specifies target gene activation, Nature 333 (1988) 185–188.

[7] M. Adachi, R. Takayanagi, A. Tomura, K. Imasaki, S. Kato, K. Goto, T. Yanase, S. Ikuyama, H. Nawata, Androgen-insensitivity syndrome as a possible coactivator disease, N. Engl. J. Med. 343 (2000) 856–862.

[8] V.V. Ogryzko, R.L. Schiltz, V. Russanova, B.H. Howard, Y. Nakatani, The transcriptional coactivators p300 and CBP are histone acetyltransferases, Cell 87 (1996) 953–959.

[9] M.L. Lu, M.C. Schneider, Y. Zheng, X. Zhang, J.P. Richie, Caveolin-1 interacts with androgen receptor. A positive modulator of androgen receptor mediated transactivation, J. Biol. Chem. 276 (2001) 13442–13451.

[10] J. Reid, I. Murray, K. Watt, R. Betney, I.J. McEwan, The androgen receptor interacts with multiple regions of the large subunit of general transcription factor TFIIF, J. Biol. Chem. 277 (2002) 41247–41253, Epub 42002 Aug 41213.

[11] X. Yu, P. Li, R.G. Roeder, Z. Wang, Inhibition of androgen receptor-mediated transcription by amino-terminal enhancer of split, Mol. Cell. Biol. 21 (2001) 4614–4625.

[12] S.A. Hayes, M. Zarnegar, M. Sharma, F. Yang, D.M. Peehl, P. ten Dijke, Z. Sun, SMAD3 represses androgen receptor-mediated transcription, Cancer Res. 61 (2001) 2112–2118.

[13] H. Dotzlaw, U. Moehren, S. Mink, A.C. Cato, J.A. Iniguez Lluhi, A. Baniahmad, The amino terminus of the human AR is target for corepressor action and antihormone agonism, Mol. Endocrinol. 16 (2002) 661–673.

[14] P.W. Hsiao, C. Chang, Isolation and characterization of ARA160 as the first androgen receptor N-terminal-associated coactivator in human prostate cells, J. Biol. Chem. 274 (1999) 22373–22379.

[15] S.M. Markus, S.S. Taneja, S.K. Logan, W. Li, S. Ha, A.B. Hittelman, I. Rogatsky, M.J. Garabedian, Identification and characterization of ART-27, a novel coactivator for the androgen receptor N terminus, Mol. Biol. Cell 13 (2002) 670–682.

[16] A. Yamamoto, Y. Hashimoto, K. Kohri, E. Ogata, S. Kato, K. Ikeda, M. Nakanishi, Cyclin E as a coactivator of the androgen receptor, J. Cell Biol. 150 (2000) 873–880.

[17] J.J. Park, R.A. Irvine, G. Buchanan, S.S. Koh, J.M. Park, W.D. Tilley, M.R. Stallcup, M.F. Press, G.A. Coetzee, Breast cancer susceptibility gene 1 (BRCA1) is a coactivator of the androgen receptor, Cancer Res. 60 (2000) 5946–5949.

[18] R.B. Lanz, N.J. McKenna, S.A. Onate, U. Albrecht, J. Wong, S.Y. Tsai, M.J. Tsai, B.W. O'Malley, A steroid receptor coactivator, SRA, functions as an RNA and is present in an SRC-1 complex, Cell 97 (1999) 17–27.

[19] Y. Zhao, K. Goto, M. Saitoh, T. Yanase, M. Nomura, T. Okabe, R. Takayanagi, H. Nawata, Activation function-1 domain of androgen receptor contributes to the interaction between subnuclear splicing factor compartment and nuclear receptor compartment. Identification of the p102 U5 small nuclear ribonucleoprotein particle-binding protein as a coactivator for the receptor, J. Biol. Chem. 277 (2002) 30031–30039, Epub 32002 May 30030.

[20] A. Nishikimi, J. Mukai, N. Kioka, M. Yamada, A novel mammalian nuclear protein similar to *Schizosaccharomyces pombe* Prp1p/Zer1p and *Saccharomyces cerevisiae* Prp6p pre-mRNA splicing factors, Biochim. Biophys. Acta 1435 (1999) 147–152.

[21] E.M. Makarov, O.V. Makarova, T. Achsel, R. Luhrmann, The human homologue of the yeast splicing factor prp6p contains multiple TPR elements and is stably associated with the U5 snRNP via protein–protein interactions, J. Mol. Biol. 298 (2000) 567–575.
[22] W. Seghezzi, K. Chua, F. Shanahan, O. Gozani, R. Reed, E. Lees, Cyclin E associates with components of the pre-mRNA splicing machinery in mammalian cells, Mol. Cell. Biol. 18 (1998) 4526–4536.
[23] K. Ishitani, T. Yoshida, H. Kitagawa, H. Ohta, S. Nozawa, S. Kato, p54nrb acts as a transcriptional coactivator for activation function 1 of the human androgen receptor, Biochem. Biophys. Res. Commun. 306 (2003) 660–665.
[24] L.D. D'Andrea, L. Regan, TPR proteins: the versatile helix, Trends Biochem. Sci. 28 (2003) 655–662.
[25] Y. Xing, C.V. Johnson, P.T. Moen Jr., J.A. McNeil, J. Lawrence, Nonrandom gene organization: structural arrangements of specific pre-mRNA transcription and splicing with SC-35 domains, J. Cell Biol. 131 (1995) 1635–1647.
[26] T. Misteli, D.L. Spector, RNA polymerase II targets pre-mRNA splicing factors to transcription sites in vivo, Mol. Cell 3 (1999) 697–705.
[27] D. Auboeuf, A. Honig, S.M. Berget, B.W. O'Malley, Coordinate regulation of transcription and splicing by steroid receptor coregulators, Science 298 (2002) 416–419.
[28] T. Misteli, Cell biology of transcription and pre-mRNA splicing: nuclear architecture meets nuclear function, J. Cell Sci. 113 (2000) 1841–1849.
[29] A. Tomura, K. Goto, H. Morinaga, M. Nomura, T. Okabe, T. Yanase, R. Takayanagi, H. Nawata, The subnuclear three-dimensional image analysis of androgen receptor fused to green fluorescence protein, J. Biol. Chem. 276 (2001) 28395–28401.
[30] M. Saitoh, R. Takayanagi, K. Goto, A. Fukamizu, A. Tomura, T. Yanase, H. Nawata, The presence of both the amino- and carboxyl-terminal domains in the AR is essential for the completion of a transcriptionally active form with coactivators and intranuclear compartmentalization common to the steroid hormone receptors: a three-dimensional imaging study, Mol. Endocrinol. 16 (2002) 694–706.
[31] A.J. Bendall, C. Abate-Shen, Roles for Msx and Dlx homeoproteins in vertebrate development, Gene 247 (2000) 17–31.
[32] J.T. Bryan, M.I. Morasso, The Dlx3 protein harbors basic residues required for nuclear localization, transcriptional activity and binding to Msx1, J. Cell Sci. 113 (2000) 4013–4023.
[33] M.M. Sohocki, S.J. Bowne, L.S. Sullivan, S. Blackshaw, C.L. Cepko, A.M. Payne, S.S. Bhattacharya, S. Khaliq, S. Qasim Mehdi, D.G. Birch, W.R. Harrison, F.F. Elder, J.R. Heckenlively, S.P. Daiger, Mutations in a new photoreceptor-pineal gene on 17p cause Leber congenital amaurosis, Nat. Genet. 24 (2000) 79–83.
[34] S. Grizot, F. Fieschi, M.C. Dagher, E. Pebay-Peyroula, The active N-terminal region of p67phox. Structure at 1.8 Å resolution and biochemical characterizations of the A128V mutant implicated in chronic granulomatous disease, J. Biol. Chem. 276 (2001) 21627–21631, Epub 22001 Mar 21621.
[35] Y. Masuhiro, Y. Mezaki, M. Sakari, K. Takeyama, T. Yoshida, K. Inoue, J. Yanagisawa, S. Hanazawa, W. O'Malley, B.S. Kato, Splicing potentiation by growth factor signals via estrogen receptor phosphorylation, Proc. Natl. Acad. Sci. USA 102 (2005) 8126–8131, Epub 2005 May 8126.
[36] D.J. Elliott, D.S. Bowman, N. Abovich, F.S. Fay, M. Rosbash, A yeast splicing factor is localized in discrete subnuclear domains, Embo J. 11 (1992) 3731–3736.
[37] T. Misteli, J.F. Caceres, D.L. Spector, The dynamics of a pre-mRNA splicing factor in living cells, Nature 387 (1997) 523–527.
[38] G. Dellaire, E.M. Makarov, J.J. Cowger, D. Longman, H.G. Sutherland, R. Luhrmann, J. Torchia, W.A. Bickmore, Mammalian PRP4 kinase copurifies and interacts with components of both the U5 snRNP and the N-CoR deacetylase complexes, Mol. Cell. Biol. 22 (2002) 5141–5156.
[39] G. Jenster, H.A. van der Korput, J. Trapman, A.O. Brinkmann, Identification of two transcription activation units in the N-terminal domain of the human androgen receptor, J. Biol. Chem. 270 (1995) 7341–7346.
[40] N.L. Chamberlain, D.C. Whitacre, R.L. Miesfeld, Delineation of two distinct type 1 activation functions in the androgen receptor amino-terminal domain, J. Biol. Chem. 271 (1996) 26772–26778.
[41] J. Reid, S.M. Kelly, K. Watt, N.C. Price, I.J. McEwan, Conformational analysis of the androgen receptor amino-terminal domain involved in transactivation. Influence of structure-stabilizing solutes and protein–protein interactions, J. Biol. Chem. 277 (2002) 20079–20086, Epub 22002 Mar 20014.
[42] R. Kumar, E.B. Thompson, Transactivation functions of the N-terminal domains of nuclear hormone receptors: protein folding and coactivator interactions, Mol. Endocrinol. 17 (2003) 1–10.

Androgen Receptor Null Male Mice Develop Late-Onset Obesity Caused by Decreased Energy Expenditure and Lipolytic Activity but Show Normal Insulin Sensitivity With High Adiponectin Secretion

WuQiang Fan,[1] Toshihiko Yanase,[1] Masatoshi Nomura,[1] Taijiro Okabe,[1] Kiminobu Goto,[1] Takashi Sato,[2] Hirotaka Kawano,[2] Shigeaki Kato,[2] and Hajime Nawata[1]

Androgen receptor (AR) null male mice ($AR^{L-/Y}$) revealed late-onset obesity, which was confirmed by computed tomography–based body composition analysis. $AR^{L-/Y}$ mice were euphagic compared with the wild-type male ($AR^{X/Y}$) controls, but they were also less dynamic and consumed less oxygen. Transcript profiling indicated that $AR^{L-/Y}$ mice had lower transcripts for the thermogenetic uncoupling protein 1, which was subsequently found to be ligand-dependently activated by AR. We also found enhanced secretion of adiponectin, which is insulin sensitizing, from adipose tissue and a relatively lower expression of peroxisome proliferator–activated receptor-γ in white adipose tissue in comparison to $AR^{X/Y}$ mice. Both factors might explain why the overall insulin sensitivity of $AR^{L-/Y}$ mice remained intact, despite their apparent obesity. The results revealed that AR plays important roles in male metabolism by affecting the energy balance, and it is negative to both adiposity and insulin sensitivity. *Diabetes* **54:1000–1008, 2005**

The etiology of obesity is extremely heterogeneous, in that it is the final result of interactions among genetic, environmental, and psychosocial factors. The androgen receptor (AR) gene may be one of these genetic factors. AR gene repeat variation was shown to be strongly associated with central obesity indexes in older adults (1). Testosterone is an important factor for determining body composition in males. Abdominal obesity is inversely correlated with serum testosterone levels in men but not in women (2). Steady increases in body fat mass accompany the age-dependent decrease in serum testosterone levels in men (3,4), leading to greater morbidity (5). Pathologically hypogonadal men also have a significantly higher fat mass (3,6), which is reversed by testosterone administration (7,8), whereas suppression of serum testosterone in healthy young men increased the percent fat mass and decreased lipid oxidation rates and resting energy expenditure (9).

We generated an AR null (ARKO) mouse line, using a Cre-loxP system (10–12), and found that male ARKO mice ($AR^{L-/Y}$) developed late-onset obesity, whereas neither heterozygous nor homozygous female ARKO mice were affected (10), suggesting a male-specific AR effect on adiposity.

Herein we report the underlying mechanism of late-onset obesity in $AR^{L-/Y}$ mice. Despite a lack of hyperphagia, $AR^{L-/Y}$ mice had lower spontaneous activity and a decreased overall oxygen consumption ratio. We also observed a concomitant decrease in expression of the thermogenic uncoupling protein 1 (UCP-1). In addition, a unique lack of insulin resistance in $AR^{L-/Y}$ mice, despite the obese phenotype, suggests it was related to an enhanced secretion of adiponectin from adipose tissue.

RESEARCH DESIGN AND METHODS

An ARKO mutant mouse line was established and maintained as described previously (10–12). Heterozygous females were bred to wild-type males (C57BL/6NCrj; Charles River Japan, Tokyo, Japan) to produce ARKO male mice ($AR^{L-/Y}$) and heterozygous females. Their diet (CLEA rodent diet CE-2; Kyudo, Tosu, Saga, Japan) had the following composition: 54.4% carbohydrate, 24.4% protein, 4.4% fat, and 342.2 kcal/100 g. Mice were weighed weekly, and food consumption was measured by weighing the remaining food every 3 days. All animal protocols were approved by the animal care and use committee of Kyushu University.

Body fat composition analysis. For computed tomography (CT) analysis of body fat composition, mice were anesthetized with intraperitoneal injections of pentobarbital sodium (Nembutal; Dainippon Pharmaceutical, Osaka, Japan) and then scanned using a LaTheta (LCT-100M) experimental animal CT system (Aloka, Tokyo, Japan). Contiguous 2-mm slice images between L2 and L4 were used for quantitative assessment using LaTheta software (version 1.00). Visceral fat, subcutaneous fat, and muscle were distinguished and evaluated quantitatively.

Spontaneous activity. Spontaneous physical activity was measured using a Letica infrared system (Panlab, Barcelona, Spain). The mice were placed in a 45 × 45 cm^2 infrared frame in which 16 × 16 intercepting infrared light beams formed a double grid of infrared cells. The position of the mice within the infrared frame was traced in a real-time manner. An additional upper infrared frame was applied to detect rearing (mouse standing up on its hind legs). Parameters such as distance traveled, speed, rearing number, and duration were analyzed using the Acti-Track program. By setting two speed thresholds

From the [1]Department of Medicine and Bioregulatory Science, Graduate School of Medical Science, Kyushu University, Fukuoka, Japan; and the [2]Institute of Molecular and Cellular Biosciences, Graduate School of Agricultural and Life Sciences, University of Tokyo, Tokyo, Japan.

Address correspondence and reprint requests to Toshihiko Yanase, MD, PhD, Department of Medicine and Bioregulatory Science, Graduate School of Medical Science, Kyushu University, Maidashi 3-1-1, Higashi-ku, Fukuoka, 812-8582 Japan. E-mail: yanase@intmed3.med.kyushu-u.ac.jp.

Received for publication 2 September 2004 and accepted in revised form 6 January 2005.

AR, androgen receptor; BAT, brown adipose tissue; CT, computed tomography; PPAR-γ, peroxisome proliferator–activated receptor-γ; UCP, uncoupling protein; WAT, white adipose tissue.

TABLE 1
List of primers

Target	Forward	Reverse	Size
UCP-2	AACAGTTCTACACCAAGGGC	AGCATGGTAAGGGCACAGTG	471
β-Actin	GCAATGCCTGGGTACATGGTGG	GTCGTACCACAGGCATTGTGATGG	492
Acetyl CoA carboxylase	GGGACTTCATGAATTTGCTGATTCTCAGTT	GTCATTACCATCTTCATTACCTCAATCTC	728
Fatty acid synthase	CACAGATGATGACAGGAGATGG	TCGGAGTGAGGCTGGGTTGAT	205
PPAR-γ coactivator 1	CGCAGCCCTATTCATTGTTC	TCATCCCTCTTGAGCCTTTC	364
Sterol regulatory element–binding protein 1c	ATCGGCGCGGAAGCTGTCGGGGTAG	ACTGTCTTGGTTGTTGATGAGCTGGAGCA	116
Leptin	TCCAGAAAGTCCAGGATGACAC	CACATTTTGGGAAGGCAGG	212
Carnitine palmitoyl transferase 1	ATTCTGTGCGGCCCTTATTGGAT	TTTGCCTGGGATGCGTGTAGTGT	395
Long-chain acyl-CoA dehydrogenase	GCTGCCCTCCTCCCGATGTT	ATGTTTCTCTGCGATGTTGATG	258
UCP-1	CACCTTCCCGCTGGACAC	CCCTAGGACACCTTTATACCTAATG	91
Hormone-sensitive lipase	CCTACTGCTGGGCTGTCAA	CCATCTGGCACCCTCACT	142
PPAR-γ	TTGACAGGAAAGACAACGGA	GAGCAGAGTCACTTGGTCATT	246
GLUT4	TCTCCAACTGGACCTGTAAC	TCTGTACTGGGTTTCACCTC	221
Muscle-type phosphofructokinase	AGATGGGTGCTAAGGCTATG	TTTTGAGGATTGGCCTCAGC	218
Muscle-type pyruvate kinase	CATTGCCGTGACTCGAAATC	CATGGTGTTGGTGAATCCAG	225
Hexokinase I	CGTGGTGCAAAAGATCCGAG	CTGCTCTTAGGCGTTCGTAG	243
Hexokinase II	TCTCAGATCGAGAGTGACTG	CGTCTCATGCATGACTTTGG	272
AR	CAGCATTATTCCAGTGGATGG	GGGCACTTGCACAGAGATG	274
UCP-1 promoter	TCCATTGGCCTCAAACCCTATGAG	AGGCGTGAGTGCAAGAACAAAAGG	3,850

of 2.00 and 5.00 cm/s, the movements were subclassified into resting (slower than 2.00 cm/s), moving slowly (between 2.00 and 5.00 cm/s), and moving fast (faster than 5.00 cm/s). The mice were placed into the frame 5 h before commencing recording to allow familiarization with the surroundings. Recording was started 2 h after the lights were switched off and lasted for 8 h; mice were assessed individually.

Oxygen consumption measurements. Mice were fed regular chow, maintained at a constant room temperature (21–23°C), and subjected to oxygen consumption measurements at ~22 weeks of age using a computer-controlled open-circuit indirect calorimeter (Oxymax; Columbus Instruments, Columbus OH). Mice were housed individually in metabolic chambers (10 × 20 cm^2) and had free access to food and water. After a 1-h adaptation to the chamber, Vo_2 was assessed at 4-min intervals for 24 h. All sample data were analyzed using Oxymax Windows software (version 1.0).

Glucose tolerance and insulin challenge tests. For the intraperitoneal glucose tolerance test, mice were fasted overnight and then injected with 2 g D-glucose/kg body wt i.p. Tail blood glucose levels were monitored before and at 15, 30, 60, 90, and 120 min after injection using blood glucose meters (Matsushita Kotobuki Electronics Industries, Ehime, Japan). For the insulin challenge test, mice were fasted overnight and then injected with 0.7 units regular insulin/kg body wt i.p. Tail blood glucose levels were measured at the same time points as above.

Histology. Mice were killed at 45 weeks old after an overnight fast, and blood was collected by cardiac puncture. Subcutaneous white adipose tissue (WAT), interscapular brown adipose tissue (BAT), liver, and kidneys were removed and immersion-fixed in 4% paraformaldehyde. After dehydration, tissue samples were paraffin-embedded in a random orientation, sliced into 10-μm sections, and stained with hematoxylin and eosin.

Blood chemicals. Blood was collected at the time of death, and the isolated serum was aliquoted and stored at −20°C until use. All blood chemistry items were measured by SRL (Tokyo, Japan). Plasma full-length adiponectin levels were measured using an enzyme-linked immunosorbent assay system as previously described (13).

Real-time PCR. Total RNA was isolated from 100 mg of intraperitoneal WAT or interscapular BAT using an RNeasy Lipid Tissue Mini Kit (Qiagen, Valencia, CA). To remove any possible DNA contamination, on-column digestion of DNA was performed with an RNase-free DNase set (Qiagen). Then, 3 μg of total RNA was subjected to reverse transcription using SuperScript III reverse transcriptase (Invitrogen, Carlsbad, CA) primed by random primers. cDNA was then subjected to real-time PCR analysis to quantify various transcripts, using a LightCycler (Roche Diagnostics, Mannheim, Germany) according to the manufacturer's instructions, as we previously described (14). The forward/reverse primer sequences for each target transcript are shown in Table 1. β-Actin was amplified simultaneously as an internal control. The real-time PCR data for each transcript were calculated as the ratio of β-actin.

UCP-1 promoter assay. A 3.85-kb (−3,860 to −10 from the start codon) region of the mouse UCP-1 promoter was amplified by PCR using specific primers (Table 1) and KOD-Plus DNA polymerase (Toyobo, Osaka, Japan) in a T-gradient thermoblock (Biometra Biomedizinische Analytik, Gottingen, Germany), and it was subsequently cloned into the pGL3-Basic (Promega, Madison, WI) vector to construct a UCP-1–Luc reporter. Direct sequencing was then performed to validate the full-length sequence and orientation. The effect of AR on the UCP-1 promoter was analyzed in NIH-3T3-L1 adipocytes by the dual luciferase assay, as described previously (15). Briefly, 1 × 10^5 cells/well were seeded into 12-well plates, and UCP-1–Luc and pCMV-AR, or pCMX (empty vector), together with the internal control pRL-CMV vector were cotransfected into the cells by SuperFect (Qiagen). The cells were incubated in 10^{-8} mol/l dihydroxytryptamine or its solvent, ethanol, for 24 h and then lysed and subjected to the relative luciferase assay using a LUMAT LB9507 luminometer (Berthold Technologies, Bad Wildbad, Germany).

Statistical analysis. Data were expressed as the means ± SD and evaluated by Student's two-tail *t* test or ANOVA, followed by post hoc comparisons with Fisher's protected least significant difference test.

RESULTS

We previously reported that up to 10 weeks old, $AR^{L-/Y}$ mice had growth retardation compared with the male wild-type ($AR^{X/Y}$) mice, but over the next couple of weeks, their body weight caught up with and then exceeded that of $AR^{X/Y}$ mice and eventually developed into overt obesity (10). These phenomena were not observed in ARKO female mice. In the present study, we performed objective CT-based body composition analysis for mice at 40 weeks of age. Figure 1*A* shows the CT-estimated weights of the adipose tissue and muscle in the area assayed (L2–L4). Although the muscle amount was unchanged, the visceral and subcutaneous fat and total fat of $AR^{L-/Y}$ mice were significantly heavier than those of $AR^{X/Y}$ mice. Figure 1*B* shows representative CT images at the L3 level of $AR^{X/Y}$ (*left*) and $AR^{L-/Y}$ (*right*) mice. $AR^{L-/Y}$ mice had increased fat in both visceral and subcutaneous areas. Thus, increased adiposity, rather than a linear increase in body growth, accounted for the elevated body weight of $AR^{L-/Y}$ mice.

The body weight of $AR^{L-/Y}$ mice at 45 weeks of age was significantly higher than that of $AR^{X/Y}$ mice (Fig. 2*A*), and, consistent with the CT data, perirenal fat pads of $AR^{L-/Y}$ mice were clearly larger that those of $AR^{X/Y}$ mice (data not shown). Despite elevated body weight, the kidneys of